INTERNATIONAL JOURNAL OF ADAPTIVE CONTROL AND SIGNAL PROCESSING
Int. J. Adapt. Control Signal Process. 2013; **00**:1–46
Published online in Wiley InterScience (www.interscience.wiley.com). DOI: 10.1002/acs

Blind Deconvolution by a Newton Method on the Non-Unitary Hypersphere

S. Fiori

Dipartimento di Ingegneria dell'Informazione, Facoltà di Ingegneria, Università Politecnica delle Marche, Via Brecce Bianche, Ancona I-60131, Italy. (eMail: s.fiori@univpm.it). Tel: +39.071.2204841, Fax:+39.071.2204224.

SUMMARY

Blind deconvolution is an inverse filtering technique that has received increasing attention from academia as well industry because of its theoretical implications and practical applications, such as in speech dereverberation, nondestructive testing and seismic exploration. An effective blind deconvolution technique is known as Bussgang, which relies on the iterative Bayesian estimation of the source sequence. Automatic gain control in blind deconvolution keeps constant the energy of the inverse filter impulse response and controls the magnitude of the estimated source sequence. The aim of the present paper is to introduce a class of Newton-type algorithms to optimize the Bussgang cost function on the inverse-filter parameter space whose geometrical structure is induced by the automatic-gain-control constraint. As the parameter space is a differentiable manifold, the Newton-like optimization method is formulated in terms of differential-geometrical concepts. The present paper also discusses convergence issues related to the introduced Newton-type optimization algorithms and illustrates their performance on a comparative basis.

Keywords: Blind deconvolution; Adaptive filtering; Criterion function optimization; Differentiable manifolds; Newton method.

Received . . .

1. INTRODUCTION

Deconvolution is a signal processing technique that aims at recovering a signal distorted by a propagation system. Deconvolution arises naturally when dealing with finite multi-path interference on a signal. In the classical formulation of the deconvolution problem, it is assumed that the system input and system output are both known (for a reference, see Figure 1). There are, however, many important physical situations where it is impractical to assume the availability of the system input, which call for a *blind deconvolution* solution. Blind deconvolution is an inverse filtering

(deconvolution) technique that does not require the knowledge of the system input nor the system's impulse response.

Blind deconvolution has received increasing attention from academia as well as industry because of its theoretical and practical implications. In speech processing, for example, blind deconvolution removes linear distortions introduced to the speech signal by the transmission channel that it propagates through [9]. Such a distortions modify the signal spectrum, as some frequency bands are amplified and other bands are attenuated and this results in unnaturally sounding speech.

A notable application of blind deconvolution is to bar code reconstruction [11]. Bar code reconstruction involves recovering a clean signal from an observed one that is corrupted by convolution with a kernel and additive noise. The form of the convolution kernel is unknown but bar codes possess a peculiar shape that facilitates their reconstruction.

Another interesting application of blind deconvolution finds in digital image integrity verification in forensics [31]. Many processing operations, both inside and outside acquisition devices, leave distinct intrinsic traces on digital images that can be identified and employed to verify the integrity of digital data. The intrinsic fingerprints of the various in-camera processing operations can be estimated through a detailed imaging model. Further processing applied to the camera-captured image is modeled as a manipulation filter, for which a blind deconvolution technique is applied to obtain a linear time-invariant estimation of the intrinsic fingerprints associated with such post-camera operations. The absence of camera-imposed fingerprints from a test image indicates that the test image is not a camera output and has possibly been generated by other image production processes. Any change or inconsistencies among the estimated camera-imposed fingerprints suggest that the image has undergone some kind of processing after the initial capture, such as tampering or steganographic embedding.

In genome biology, a blind deconvolution approach to high-resolution mapping of transcription factor binding sites was proposed [22]. Such computational method determines locations of transcription factor binding. The use of a blind deconvolution approach allows closely-spaced binding sites to be called accurately.

Three-dimensional laser radar sensors are unique due to the ability to rapidly acquire a series of two-dimensional remote scene data. Principal causes of laser radar range estimation error include spatial blur, detector blurring, noise and timing jitter. The research work [23] accounts for pixel coupling by defining the mathematical model of the range-image by two-dimensional convolution between the spatial impulse response of the propagation system and the object (target or remote scene) at a particular point in time. Using such model, improved range estimation is possible by object restoration from the observations by a blind deconvolution algorithm.

Advanced nondestructive testing techniques use a laser to generate ultrasonic waves at the surface of a specimen under test. An air-coupled transducer receives the ultrasound that results from the

Prepared using acsauth.cls
DOI: 10.1002/acs

convolution of the signal leaving the test material and the distortion function. Blind deconvolution methods are then applied to estimate the signal leaving the material [24].

In marine seismic exploration, the aim is to obtain an image of the sea bottom lithography from reflected acoustic waves emitted by various seismic sources [25]. In seismic deconvolution, blind approaches must be considered in situations where the reflectivity sequence, the source wavelet signal and the noise power level are unknown.

Thin films are applied in optical detection and modulation sensors. As these films exhibit hysteresis in the temperature-resistance characteristic, their thermodynamic characterization is required. Temperature sensors present slow dynamic responses, and thus, when characterizing thermal hysteresis, the result is a distorted version of the real curve. One way to avoid such problem is to perform thermodynamic characterization by applying a very low temperature ramp. Such procedure is time-consuming and cannot be repeated for a large number of films. Paper [12] discusses an unsupervised signal processing procedure to remove the distortion introduced by the measurement channel. To this aim, a blind deconvolution algorithm is applied to estimate both the measurement channel and the real temperature signal, using only the measured temperature.

Fault diagnosis and failure prognosis are essential techniques in improving the safety of mechanical systems. The performance of vibration-based diagnostic and prognostic algorithms is degraded by the presence of noise in the vibration signals. The contribution [34] proposes a denoising method based on a blind deconvolution technique and applies such method to the concrete case of the analysis of vibration signals collected from a test-bed of an helicopter's main gearbox subjected to a seeded fault.

Further notable applications of blind deconvolution are to optomagnetic memory-support storage and retrieval enhancement [6] and retinal image deconvolution [33].

An effective blind-deconvolution technique is known as 'Bussgang'. It relies on the iterative Bayesian estimation of the source sequence, where the (approximate) Bayesian estimator is matched to source statistics and to the model of the deconvolving filter output signal (see, e.g., [13, 15]). The Bussgang method may be formulated in terms of a cost function that describes the performance of a linear inverse filter. Automatic gain control in blind deconvolution keeps constant the energy of the inverse-filter impulse response sequence and hence controls the magnitude of the estimated source sequence. Automatic gain control induces a differentiable-manifold structure in the inverse-filter parameter space.

The aim of the present contribution is to discuss a class of Newton-type algorithms to optimize the Bussgang cost function on the parameter space whose geometrical nature is induced by the automatic gain control constraint. In numerical analysis, Newton's method is used for finding successively better approximations to the zeroes of a real-valued function. Newton's method may be used to find critical points of differentiable functions in the unconstrained setting [27] as well as

DOI: 10.1002/acs

in the constrained case [3, 27]. In the case of interest in the present paper, the parameter space is a differentiable manifold, therefore the Newton-like optimization method is to be formulated in terms of differential-geometrical concepts [18].

The numerical implementation of a Newton-like optimization method on a computation platform requires notions from geometric numerical integration [20]. The present paper builds on the previous contributions [13, 17]. The present contribution introduces the following new topics:

- A Newton-like stepping method to optimize the Bussgang cost function on the parameter manifold. The presented algorithm is general in the sense that the stepping method on the manifold of interest is formulated in terms of a generic retraction map, hence generalizing results known in the related literature [18, 32].
- A convergence analysis for the Newton-like optimization algorithm on manifolds which is suitable for generic manifolds and generic retraction maps, which generalize results known from the related literature [18, 32].

The present manuscript is organized as follows. Section 2 summarizes the basics of blind signal deconvolution by the 'Bussgang' method. Section 3 recalls the notion of optimization by Newton method on manifolds. In particular, subsection 3.1 recalls the familiar gradient-steepest-descent and damped-Newton methods on the Euclidean space $\mathbb{R}^n$; subsection 3.2 then recalls notions from differential geometry that are instrumental in the development of the subsequent analysis; subsection 3.3 explains the counterparts of gradient-steepest-descent method and of the damped-Newton method on differentiable manifolds; subsection 3.4 particularizes the general-purpose results of subsection 3.3 to the case of the non-unitary hypersphere. Section 4 discusses in detail the convergence issues related to the retracted-Riemannian-gradient and the retracted-Riemannian-Newtonian algorithms. In particular, subsection 4.1 recalls the convergence analysis for the Newton's algorithm on Euclidean spaces as a basis for the convergence analysis of the retracted-damped-Newtonian algorithm on manifolds carried out in subsection 4.3, while subsection 4.2 briefly discusses the convergence of the retracted-Riemannian-gradient algorithm on manifolds. Section 5 presents the results of numerical experiments on a real-world channel, both noiseless and noisy, as well as a comparative analysis that takes as reference blind deconvolution algorithms known from the literature. Section 6 concludes the paper.

2. BLIND DECONVOLUTION BY BAYESIAN ESTIMATION

The present section recalls the distorting system model as well as the inverse-filter model used throughout this paper (subsection 2.1) and the main features of blind deconvolution by Bayesian estimation theory (subsection 2.2). It also recalls the notion of *automatic gain control* in adaptive

Prepared using acsauth.cls
DOI: 10.1002/acs

filtering and introduces the optimization problem related to blind deconvolution (subsection 2.3). General purpose references on blind deconvolution theory are, e.g., [2, 9].

2.1. *System-filter models*

The linear discrete-time time-invariant system to deconvolve, as depicted in the Figure 1, is described by the following input/output model:

$$b_\tau = \sum_{u=0}^{L_h-1} h_u s_{\tau-u} + \mathcal{N}_\tau,\ \tau = 0, 1, 2, \ldots, \tag{1}$$

where quantity h_τ denotes system's impulse response of finite length L_h, symbol s_τ denotes the system's input stream and $\mathcal{N}_\tau$ represents a zero-mean white measurement disturbance independent of the source signal. The system's impulse response satisfies $\sum_\tau h_\tau^2 = 1$ and its inverse has finite energy. The source signal s_τ is a stationary, ergodic, independent identically distributed (IID) random process with zero mean and bounded variance. Also, the probability density function of the source signal is symmetric around zero and non-Gaussian.

An adaptive filter is the approximate inverse of system (1) if it approximately cancels the effects of the distorting system on the source signal. The output stream of the adaptive filter at optimization step k computes as:

$$z_{k,\tau} = \sum_{\tau=0}^{L_x-1} x_{k,u} b_{\tau-u},\ \tau = 0, 1, 2, \ldots,\ k = 0, 1, 2, \ldots, \tag{2}$$

where quantity $x_{k,\tau}$ denotes inverse-filter's impulse response of finite length L_x at adaptation step k. Throughout the paper, the subscript τ denotes sample index while the subscript k denotes the optimization step/iteration-number.

The system noise $\mathcal{N}_\tau$ in the model (3) is assumed to be weak: Bussgang-type blind deconvolution theory was developed to reduce the inter-symbol interference primarily and cannot cope with low signal-to-noise ratios [1]. In practice, this means that the additive system noise is supposed to have been reduced by noise-filtering the system output signal beforehand. The hypotheses made on the convolution process imply that the inverse problem to be solved is well-posed. In some applied area, however, the above basic hypotheses might not be met: In seismic applications, for instance, the noise level can be quite strong and convolution might be band-limited, hence, non-invertible. There appears to exist few contributions dealing with the above difficulties [21, 26].

The system's impulse response zeros are assumed to lie sufficiently far away from the unit circle in the complex plane (namely, no 'deep zeros' affect the system, [1]). Deep zeros in a system impulse response would make it necessary to adopt a deconvolving filter whose impulse response should be very long, which would make FIR filtering unsuitable. In this case, IIR filtering would be appropriate, as proposed in [4, 16]. Provided that zeros close to the unit circle are excluded, the

Prepared using acsauth.cls
DOI: 10.1002/acs

system's zeros may lie both inside and out-side the unit circle, meaning that minimum-phase as well as non-minimum phase systems deconvolution may be tackled within the Bussgang framework.

2.2. *Bussgang filtering*

In general, deconvolution may only be approximate because of the additive noise affecting the system's output measure and because a finite-impulse-response (FIR) filter cannot represent the inverse of the FIR system (1). Since the impulse response of the distorting system as well as the source stream are unknown, the optimal filter-tap-weights $x_{\star,\tau}$ such that signal $z_{\star,\tau}$ is an accurate estimate of signal s_τ can be identified by means of a *blind* adaptive algorithm. During filter adaptation, the misadjustment of filter's coefficients makes filter's output differ from the source signal. Filter misadjustment, additive noise and FIR-by-FIR inversion difficulty may be accounted for through the following filter-output signal model:

$$z_{k,\tau} = c_k s_{\tau-\Delta_k} + \nu_{k,\tau},\ \tau = 0, 1, 2, \ldots,\ k = 0, 1, 2, \ldots, \tag{3}$$

where the sequence $\nu_{k,\tau}$ represents the so-called *deconvolution noise*, the variable $c_k \in \mathbb{R}$ denotes instantaneous amplitude distortion and the quantity Δ_k denotes group delay. A commonly used representation of noise $\nu_{k,\tau}$ is a zero-mean, white, Gaussian random process uncorrelated with the source signal. The model (3) reveals that the relationship between the signal $z_{k,n}$ and the signal $c_k s_{\tau-\Delta_k}$ is deterministic but for the deconvolution noise, therefore, an appropriate estimator of the source sequence having form $A(z_{k,\tau})$ can be designed according to Bayesian estimation theory. On the basis of the available Bayesian estimator, in [1] the following error criterion had been proposed:

$$C(x_{k,0}, x_{k,1}, \ldots, x_{k,L_x-1}) \stackrel{\text{def}}{=} \frac{1}{2}\mathfrak{E}_\tau[\nu_{k,\tau}^2] = \frac{1}{2}\mathfrak{E}_\tau\left[(z_{k,\tau} - A(z_{k,\tau}))^2\right], \tag{4}$$

where symbol $\mathfrak{E}[\cdot]$ denotes temporal average. The minimization of the above cost function may be achieved by a stochastic least-mean-square algorithm, as in [1], by means of a stochastic gradient steepest descent algorithm, as in [13], or by any other suitable known optimization method.

Bussgang filtering theory allows computing the expression of the Bayesian estimator given the source stream probability density function [13]. In the case of uniformly distributed source stream, which is of interest, e.g., in telecommunication systems, a suitable approximation of the actual Bayesian estimator was described and studied in [13]. In the contribution [14], a batch procedure was proposed in order to optimize the approximation of the actual Bayesian estimator, an extensive analysis of which is available in [15].

2.3. *Automatic gain control and vector notation*

Paper [13] invokes the automatic gain control (AGC) constraint. AGC aims at keeping constant the energy of the filter impulse response sequence, that means enforcing the constraint $\sum_{\tau=0}^{L_x-1} x_{k,\tau}^2 = \varrho^2$, with $\varrho > 0$ being the filter gain.

Prepared using acsauth.cls
DOI: 10.1002/acs

Introducing the weight-vector notation $x \in \mathbb{R}^{L_x}$ for the adaptive filter, the adaptation algorithm that seeks for the minimum of the Bussgang criterion function $C(x_k)$ must ensure that, at any step k, it holds that:

$$x_k \in \left\{ x \in \mathbb{R}^{L_x} \,\middle|\, x^T x = \varrho^2 \right\}, \tag{5}$$

where superscript ^{T} denotes vector transpose. The above set is termed *non-unitary hypersphere*, which possesses the structure of a curved differentiable manifold. The Newton-like optimization algorithm that adapts filter's tap-weights of interest in the present paper must be designed in a way that ensures that the above constraint is met at any step of optimization.

Note that, extending the vector notation to the adaptive filter input, namely, defining:

$$x_k \stackrel{\text{def}}{=} [x_{k,0} \; x_{k,1} \; \ldots \; x_{k,L_x-1}]^T, \tag{6}$$

$$\bar{b}_\tau \stackrel{\text{def}}{=} [b_\tau \; b_{\tau-1} \; \ldots \; b_{\tau-L_x+1}]^T, \tag{7}$$

with appropriate zero-padding, then it holds that $z_{k,\tau} = x_k^T \bar{b}_\tau$ and hence:

$$C(x_k) = \frac{1}{2} \mathfrak{E}_\tau \left[\left(x_k^T \bar{b}_\tau - A(x_k^T \bar{b}_\tau) \right)^2 \right]. \tag{8}$$

The design of a Newton-like optimization algorithm that adapts filter's weight-vector is discussed in the following section.

3. NEWTONIAN OPTIMIZATION METHOD ON MANIFOLDS

Newton's method was developed to find the roots of a polynomial and has since then been generalized in different ways [27]. The present section begins by recalling the familiar gradient-based and Newton-type optimization methods on the Euclidean space $\mathbb{R}^n$ (subsection 3.1) and proceeds by explaining how such methods may be extended to the case of optimization on curved spaces that possess the structure of Riemannian manifolds (subsection 3.3). Subsection 3.2 recalls notions from differential geometry which are instrumental in the development of optimization methods on Riemannian manifolds as well as in the discussion of their convergence properties. Note that the optimization algorithms discussed within the present section are formulated in general terms, with an exception of subsection 3.4, which deals with the special case of the non-unitary hypersphere of particular interest in the context of blind deconvolution.

3.1. Gradient method and Newton's method on the space $\mathbb{R}^n$

Let $F : \mathbb{R}^n \to \mathbb{R}$ be a regular function endowed with a minimum at $x^\star \in \mathbb{R}^n$. Symbol $\partial_x F \in \mathbb{R}^n$ denotes the Euclidean gradient of the function F at $x \in \mathbb{R}^n$ and symbol $\partial_x^2 F \in \mathbb{R}^{n \times n}$ denotes the Hessian of the function F at $x \in \mathbb{R}^n$. The Hessian matrix is symmetric and positive-definite at the point $x^\star$.

Prepared using acsauth.cls
DOI: 10.1002/acs

Given any initial guess $x \in \mathbb{R}^n$ of the critical point $x^\star$, a more accurate estimate $y \in \mathbb{R}^n$, may be found by defining an approximation of function F around the point x through a Taylor expansion truncated to the first-order term, namely:

$$\tilde{F}(y) \stackrel{\text{def}}{=} F(x) + (y-x)^T \partial_x F, \tag{9}$$

where superscript ^{T} denotes transpose. The best approximation $y \in \mathbb{R}^n$ according to the above linear approximation minimizes $\tilde{F}(y)$ under the condition that $(y-x)^T(y-x) = \epsilon^2$, with $\epsilon > 0$ fixed and sufficiently small. Define the Lagrangian function:

$$L(y) \stackrel{\text{def}}{=} \mu((y-x)^T(y-x) - \epsilon^2) + (y-x)^T \partial_x F, \tag{10}$$

where $\mu \in \mathbb{R}$ denotes a Lagrangian multiplier. The point y such that the function $\tilde{F}(y)$ attains its minimum value, under the constraint that y is not too far from x satisfies the condition $\partial_y L(y) = 0$. As it holds $\partial_y L(y) = 2\mu(y-x) + \partial_x F$, the *direction* along which the difference $F(x) - \tilde{F}(y)$ decreases the most is given by $-\partial_x F$, hence the best estimate y upon the linear approximation (9) writes:

$$\left\{ \begin{array}{l} y = x + tv, \\ v = -\partial_x F, \end{array} \right. \tag{11}$$

with $t > 0$. The geometric interpretation of the system (11), which explains the essence of gradient-steepest-descent method, is that, to attain a better estimate than x, move from x along a straight line in the direction v of an extent t, where v is the direction of steepest descent. The parameter t is oftentimes referred to as *optimization stepsize*. The value $t^\star$ of the optimal stepsize may be fixed by solving an optimization subproblem, for instance:

$$t^\star \stackrel{\text{def}}{=} \arg\min_{t>0} \{F(x+tv)\}, \tag{12}$$

that is well-defined as long as the initial guess x does not coincide with the minimum $x^\star$. In fact, observe that, under such condition:

$$\frac{d}{dt} F(x+tv)\bigg|_{t=0} = v^T \partial_x F = -\|\partial_x F\|^2 < 0, \tag{13}$$

hence, by continuity, there exists some $t > 0$ for which $F(x+tv) < F(x)$.

The method (11) may be used iteratively to refine the initial guess and gives rise to the iterative optimization algorithm:

$$x_{k+1} = x_k - t_k \partial_{x_k} F, \tag{14}$$

where $t_k > 0$ denotes an optimization stepsize schedule and $k \in \mathbb{N}$. The point $x_0 \in \mathbb{R}^n$ denotes an initial guess.

Another way of determining a more accurate estimate $y \in \mathbb{R}^n$ of the minimum of the criterion function F than the initial guess $x \in \mathbb{R}^n$ is to define an approximation of the criterion function F

Prepared using acsauth.cls
DOI: 10.1002/acs

around the point x through a Taylor expansion truncated to the second-order term. Likewise the gradient-steepest-descent method, one fixes the way of moving from the initial guess x to the new estimate y along a straight line $y = x + tv$ and looks for the direction v that corresponds to the largest change of the value of the function F, namely, that minimizes the function:

$$\bar{F}(v) \stackrel{\text{def}}{=} F(x) + v^T \partial_x F + \frac{1}{2} v^T \partial_x^2 F v. \tag{15}$$

Note that the truncated Taylor expansion (15) is formulated in terms of the direction v already. Also, note that if the Hessian map $x \mapsto \partial_x^2 F$ enjoys some regularity condition (for example, Lipschitz continuity), then in a neighborhood of the critical point $x^\star$ the Hessian $\partial_x^2 F$ is symmetric positive-definite and hence invertible. The direction $v \in \mathbb{R}^n$ that minimizes $\bar{F}(v)$ satisfies the condition:

$$\partial_v \bar{F} = 0. \tag{16}$$

As it holds $\partial_v \bar{F}(v) = \partial_x F + \partial_x^2 F v$, the condition (16) gives rise to the system:

$$\begin{cases} y = x + tv, \\ v = (\partial_x^2 F)^{-1}(-\partial_x F), \end{cases} \tag{17}$$

where $(\partial_x^2 F)^{-1}$ denotes the inverse of the Hessian matrix of the function F evaluated at x and $t > 0$. The system (17) is commonly referred to as (damped) Newton's method [27]. The case $t = 1$ corresponds to the Newton's method, while in a damped Newtonian iteration the optimal value of the stepsize may be selected by solving the optimization subproblem:

$$t^\star \stackrel{\text{def}}{=} \arg \min_{0 < t \leq 1} \{F(x + tv)\}. \tag{18}$$

The stepsize selection rule (18) is well-defined as long as the initial guess x does not coincide with the minimum $x^\star$. In fact, observe that, under such condition:

$$\frac{d}{dt} F(x + tv)\Big|_{t=0} = -(\partial_x F)^T (\partial_x^2 F)^{-1} \partial_x F < 0, \tag{19}$$

hence, by continuity, there exists some $t > 0$ such that $F(x + tv) < F(x)$.

The method (17) may be used iteratively to refine the initial guess and gives rise to the iterative optimization algorithm:

$$x_{k+1} = x_k - t_k (\partial_{x_k}^2 F)^{-1} \partial_{x_k} F, \tag{20}$$

where $t_k \in (0\ 1]$ denotes an optimization stepsize schedule and $k \in \mathbb{N}$. The point $x_0 \in \mathbb{R}^n$ denotes an initial guess to be selected sufficiently close to $x^\star$ for the algorithm to converge.

In order to extend the above optimization methods to seek for a minimum of a differentiable function $F : M \to \mathbb{R}$ defined on a differentiable manifold M, it is necessary to replace the notion of 'moving on a straight line' with the notion of 'moving on a geodesic arc', to extend the notion of first-order and second-order Taylor expansions in $\mathbb{R}^n$ by the notions of Riemannian gradient and Riemannian Hessian tensor, and to extend the step-wise optimality condition (16). Such extensions require instruments from differential geometry that are recalled in the next subsection.

Prepared using acsauth.cls
DOI: 10.1002/acs

3.2. Notions of differential geometry

The present subsection recalls notions from differential geometry that are instrumental in the development of a theory of Newton-like optimization on manifolds. For the theory of differentiable manifolds, readers may refer to [29].

Let M be a differentiable manifold of dimension n and $\mathbb{E}^n$ denote the Euclidean space of dimension n that the manifold M is embedded within. At a point $x \in M$, the tangent space to the manifold M is denoted as T_xM. Each tangent space T_xM is a differentiable manifold itself, of the same dimension of the space M. The symbol TM denotes the tangent bundle of the manifold M and is defined as $TM \stackrel{\text{def}}{=} \{(x,v) | x \in M, v \in T_xM\}$.

A Riemannian manifold M is endowed with a inner product $\langle \cdot, \cdot \rangle_x : T_xM \times T_xM \to \mathbb{R}$. The inner product $\langle \cdot, \cdot \rangle_x$ is a positive bilinear form and a smooth function of x that induces the norm $\|v\|_x \stackrel{\text{def}}{=} \sqrt{\langle v, v \rangle_x}$ in every tangent space $T_xM \ni v$. The Euclidean inner product has a spacial place in geometry and is hereafter denotes as $\langle \cdot, \cdot \rangle^{\mathrm{E}} : \mathbb{E}^n \times \mathbb{E}^n \to \mathbb{R}$. The Euclidean norm of an element $x \in \mathbb{E}^n$ is denoted and defined as $\|x\| \stackrel{\text{def}}{=} \sqrt{\langle x, x \rangle^{\mathrm{E}}}$.

A smooth parametric curve in the manifold M maps an interval $[-a\ a] \subset \mathbb{R}$ to M and is denoted by $c : [-a\ a] \to M$, with $a > 0$. The notation $c_{x,v}(t)$, with $(x,v) \in TM$, is used to specify a curve such that $c_{x,v}(0) = x \in M$ and $\dot{c}_{x,v}(0) = v \in T_xM$.

Let $\mathfrak{X}(M)$ denote the set of vector fields of the manifold M. A vector field $\mathcal{W} \in \mathfrak{X}(M)$ on a manifold M is a smooth map $\mathcal{W} : x \in M \mapsto \mathcal{W}(x) \in T_xM$. Given a point $x \in M$, a vector $v \in T_xM$ and a vector field $\mathcal{W} \in \mathfrak{X}(M)$, symbol $\nabla_v \mathcal{W}$ denotes the covariant derivative of $\mathcal{W}$ along v. The covariant derivative of a vector field along a vector describes the amount of change of the vector field in a given direction. The covariant derivative is also termed *connection*. Let $\mathcal{V}, \mathcal{W} \in \mathfrak{X}(M)$, the covariant derivative of $\mathcal{W}$ with respect to $\mathcal{V}$ defines an operator $\nabla : \mathfrak{X}(M) \times \mathfrak{X}(M) \to \mathfrak{X}(M)$ specified by $(\nabla_{\mathcal{V}} \mathcal{W})(x) \stackrel{\text{def}}{=} \nabla_{\mathcal{V}(x)} \mathcal{W}$.

Any smooth parametric curve $c : [-a\ a] \to M$ defines a parameterized velocity vector field $\dot{c}(t) \in T_{c(t)}M$. A vector field $\mathcal{W} \in \mathfrak{X}(M)$ defines, by restriction, a parameterized vector field $w(t) \stackrel{\text{def}}{=} \mathcal{W}(c(t)) \in T_{c(t)}M$ along the curve $c(t) \in M$. A vector field $\mathcal{W} \in \mathfrak{X}(M)$ is said to be *parallel along the curve* $c(t)$ if its covariant derivative along the velocity vector field $\dot{c}(t)$ is identically zero, namely $\nabla_{\dot{c}(t)} \mathcal{W} = 0$ for any t. By introducing the Christoffel form $\Gamma_x : T_xM \times T_xM \to \mathbb{E}^n$, the equation that states the parallelism of a vector field along a curve writes:

$$\dot{w}(t) + \Gamma_{c(t)}(\dot{c}(t), w(t)) = 0, \tag{21}$$

where $w(t)$ denotes the restriction of the vector field $\mathcal{W}$ to the curve $c(t)$. Given a smooth parameterized curve $c : [-a\ \ a] \to M$, for each vector $v \in T_{c(0)}M$ there exists a unique parameterized parallel vector field $w(t)$ along $c(t)$ such that $w(0) = v$. The Christoffel form is not

DOI: 10.1002/acs

uniquely specified for a given manifold but a special form, that depends only on manifold's metrics, is known and gives rise to the Levi-Civita connection.

Given a smooth manifold M, a smooth curve $c : [-a\ a] \to M$ with $c(0) = x \in M$ and a tangent vector $v \in T_x M$, the notion of parallelism provides a way to move the vector v along the curve c in a way that keeps the translated vector parallel to the curve. In fact, the differential equation (21) with initial condition $w(0) = v$, defines a curve $t \mapsto w(t) \in T_{c(t)}M$ that is a restriction of a parallel vector field $\mathcal{W}$. The parallel translation of a given tangent vector along a curve $c(t)$ is expressed through an operator $\Gamma(c)_\theta^t : T_{c(\theta)}M \to T_{c(t)}M$ termed *parallel translation* operator. The parallel translation operator is such that:

- The map $\Gamma(c)_t^t$ coincides with the identity map in $T_{c(t)}M$,
- The composition law $\Gamma(c)_\sigma^t \circ \Gamma(c)_\theta^\sigma = \Gamma(c)_\theta^t$ holds,
- The operator $\Gamma(c)_\theta^t$ depends smoothly on parameters θ and t.

Given a smooth manifold M, a vector field $\mathcal{V} \in \mathfrak{X}(M)$, a pair $(x, v) \in TM$ and a parallel-translation operator Γ, the covariant derivation on M may be defined as follows. Let $c_{x,v} : [-a\ a] \to M$ denote a smooth curve, then:

$$\nabla_v \mathcal{V} = \lim_{t\to 0} \frac{\Gamma(c_{x,v})_t^0 \mathcal{V}(c_{x,v}(t)) - \mathcal{V}(x)}{t} = \frac{d}{dt}\Gamma(c_{x,v})_t^0 \mathcal{V}(c_{x,v}(t))\Big|_{t=0}. \tag{22}$$

The Levi-Civita connection defines a *metric* parallel translation, namely it holds:

$$\langle \Gamma(c)_\theta^t v, \Gamma(c)_\theta^t w\rangle_{c(t)} = \langle v, w\rangle_{c(\theta)}, \tag{23}$$

for all $v, w \in T_{c(\theta)}M$, as illustrated in the Figure 2. Namely, a metric parallel translation preserves the angle between any two tangent vectors.

Let $c : [-a\ a] \to M$ denote a smooth curve on the smooth manifold M endowed with the parallel translation Γ and let $\mathcal{V} \in \mathfrak{X}(M)$. The following identity holds:

$$\frac{d}{dt}\Gamma(c)_t^0 \mathcal{V}(c(t)) = \Gamma(c)_t^0 \nabla_{\dot{c}(t)} \mathcal{V}. \tag{24}$$

It may be proven by recalling the definition:

$$\frac{d}{dt}\Gamma(c)_t^0 \mathcal{V}(c(t)) = \lim_{\epsilon\to 0} \frac{\Gamma(c)_{t+\epsilon}^0 \mathcal{V}(c(t+\epsilon)) - \Gamma(c)_t^0 \mathcal{V}(c(t))}{\epsilon} \tag{25}$$

and making use of the decomposition $\Gamma(c)_{t+\epsilon}^0 = \Gamma(c)_t^0 \circ \Gamma(c)_{t+\epsilon}^t$, that implies:

$$\frac{d}{dt}\Gamma(c)_t^0 \mathcal{V}(c(t)) = \Gamma(c)_t^0 \lim_{\epsilon\to 0} \frac{\Gamma(c)_{t+\epsilon}^t \mathcal{V}(c(t+\epsilon)) - \mathcal{V}(c(t))}{\epsilon}. \tag{26}$$

From equation (22) if follows that the limit in the equation (26) equals the covariant derivative $\nabla_{\dot{c}(t)}\mathcal{V}$.

Let M and N be two differentiable manifolds and $F : M \to N$ a smooth map between them. The map F induces a map between the tangent bundles TM and TN termed *tangent map*. The tangent

DOI: 10.1002/acs

map associated to $F : M \to N$ is expressed as $dF|_x : T_xM \to T_{F(x)}M$. Let $c_{x,v} : [-a\ a] \to M$ be a smooth curve and consider the map $t \mapsto F(c_{x,v}(t))$. Set $w \stackrel{\text{def}}{=} \frac{d}{dt}F(c_{x,v}(t))\big|_{t=0}$. By the composition law of derivatives, the velocity vector field of the curve $F(c_{x,v}(t))$ may be expressed as:

$$\frac{d}{dt}F(c_{x,v}(t)) = dF|_{c_{x,v}(t)}\left(\frac{d}{dt}c_{x,v}(t)\right). \tag{27}$$

Setting $t = 0$ gives $w = dF|_x(v)$. (The tangent map $dF|_x$ is also termed *pushforward*.)

A parameterized curve $c : [-a\ a] \to M$ is termed *geodesic* if its own velocity vector field is parallel along $c(t)$, namely, if $\nabla_{\dot{c}}\dot{c} = 0$. In terms of the Christoffel form, the geodesic equation writes:

$$\ddot{c}(t) + \Gamma_{c(t)}(\dot{c}(t), \dot{c}(t)) = 0. \tag{28}$$

Given $(x, v) \in TM$, there exists a unique solution of the geodesic equation (28) with initial conditions $c(0) = x$ and $\dot{c}(0) = v$, denoted by $\gamma_{x,v}(t)$. Geodesic arcs generalize the notion of 'straight lines' in Euclidean spaces, in fact, they possess the distinguishing feature of being self-parallel. Given a geodesic curve $\gamma_{x,v}(t)$, apply identity (24) to the velocity vector field $\mathcal{V}(\gamma_{x,v}(t)) \stackrel{\text{def}}{=} \dot{\gamma}_{x,v}(t)$. The result is:

$$\frac{d}{dt}\Gamma(\gamma_{x,v})_t^0\dot{\gamma}_{x,v}(t) = \Gamma(\gamma_{x,v})_t^0\nabla_{\dot{\gamma}_{x,v}(t)}\dot{\gamma}_{x,v}(t) = 0, \tag{29}$$

which leads to the self-parallel-translation identity:

$$\Gamma(\gamma_{x,v})_t^0\dot{\gamma}_{x,v}(t) = \Gamma(\gamma_{x,v})_0^0\dot{\gamma}_{x,v}(0) = v, \tag{30}$$

or, equivalently:

$$\dot{\gamma}_{x,v}(t) = \Gamma(\gamma_{x,v})_0^t v. \tag{31}$$

The notion of geodesics turns a manifold into a metric space. Given a geodesic arc $\gamma_{x,v} : [0\ 1] \to M$ on a Riemannian manifold M, the distance between its endpoints, namely $x = \gamma_{x,v}(0)$ and $y \stackrel{\text{def}}{=} \gamma_{x,v}(1)$, is defined as:

$$\delta(x, y) \stackrel{\text{def}}{=} \int_0^1 \sqrt{\langle\dot{\gamma}_{x,v}(\theta), \dot{\gamma}_{x,v}(\theta)\rangle_{\gamma_{x,v}(\theta)}}d\theta. \tag{32}$$

If the manifold M is endowed with a Levi-Civita connection that corresponds to a metric parallel translation operator, the properties (23) and (31) hold together and give:

$$\delta(x, y) = \int_0^1 \sqrt{\langle\Gamma(\gamma_{x,v})_0^\theta v, \Gamma(\gamma_{x,v})_0^\theta v\rangle_{\gamma_{x,v}(\theta)}}d\theta = \int_0^1 \sqrt{\langle v, v\rangle_x}d\theta = \|v\|_x. \tag{33}$$

Let $F : M \to \mathbb{R}$ denote a differentiable function. Symbol $\nabla_x F \in T_xM$ denotes the Riemannian gradient of function F with respect to a metric $\langle\cdot,\cdot\rangle_x$ while symbol $\nabla_x^2 F$ denotes the Riemannian Hessian of function F with respect to the metric $\langle\cdot,\cdot\rangle_x$. Given any smooth parametric curve $c_{x,v} : [-a\ a] \to M$, the Riemannian gradient of function $F : M \to \mathbb{R}$ with respect to a metric $\langle\cdot,\cdot\rangle_x$

Prepared using acsauth.cls
DOI: 10.1002/acs

is the unique tangent vector that satisfies the condition:

$$\langle \nabla_x F, v \rangle_x = \left. \frac{dF(c_{x,v}(t))}{dt} \right|_{t=0}, \text{ for all } v \in T_x M. \tag{34}$$

Note that:

$$\frac{dF(c_{x,v}(t))}{dt} = \langle \partial_{c_{x,v}(t)} F, \dot{c}_{x,v}(t) \rangle^{\mathrm{E}}, \tag{35}$$

therefore, setting $t = 0$, yields:

$$\langle \nabla_x F, v \rangle_x = \langle \partial_x F, v \rangle^{\mathrm{E}}, \ \forall v \in T_x M, \tag{36}$$

which is known as *metric compatibility condition* and provides an operative definition of the Riemannian gradient. The last equality shows that the Riemannian gradient does not depend on the choice of the curve $c_{x,v}(t)$ but it depends on the chosen metric $\langle \cdot, \cdot \rangle_x$. Note that the Riemannian gradient on a manifold M defines a vector field $\mathcal{G} \overset{\text{def}}{=} \nabla F \in \mathfrak{X}(M)$ such that $\mathcal{G}(x) = \nabla_x F$ for all $x \in M$. The Riemannian Hessian of function $F : M \to \mathbb{R}$ with respect to a metric $\langle \cdot, \cdot \rangle_x$ applied to a vector $v \in T_x M$ is the unique tangent vector that satisfies the condition:

$$\langle \nabla_x^2 F(v), v \rangle_x = \left. \frac{dF^2(c_{x,v}(t))}{dt^2} \right|_{t=0}, \text{ for all } v \in T_x M. \tag{37}$$

The Riemannian Hessian may be regarded as a *linear* operator $\nabla_x^2 F : T_x M \to T_x M$, hence the quantity $\langle \nabla_x^2 F(v), v \rangle_x$ is quadratic in v. The Riemannian Hessian does not depend on the curve $c_{x,v}$ in (37), hence it may be assumed $c_{x,v} = \gamma_{x,v}$. Also, note that in a generic Euclidean space $\mathbb{E}^n$ the Hessian $\partial_x^2 F : \mathbb{E}^n \to \mathbb{E}^n$ of a function $F : \mathbb{E}^n \to \mathbb{R}$ at $x \in \mathbb{E}^n$ is an operator hence it is customary to adopt the notation $\partial_x^2 F(v)$ with $v \in T_x \mathbb{E}^n \cong \mathbb{E}^n$. It holds that:

$$\begin{aligned} \frac{d^2 F(\gamma_{x,v}(t))}{dt^2} &= \langle \frac{d}{dt} \partial_{\gamma_{x,v}(t)} F, \dot{\gamma}_{x,v}(t) \rangle^{\mathrm{E}} + \langle \partial_{\gamma_{x,v}(t)} F, \ddot{\gamma}_{x,v}(t) \rangle^{\mathrm{E}}, \\ &= \langle \partial^2_{\gamma_{x,v}(t)} F(\dot{\gamma}_{x,v}(t)), \dot{\gamma}_{x,v}(t) \rangle^{\mathrm{E}} + \\ &\quad \langle \partial_{\gamma_{x,v}(t)} F, -\Gamma_{\gamma_{x,v}(t)}(\dot{\gamma}_{x,v}(t), \dot{\gamma}_{x,v}(t)) \rangle^{\mathrm{E}}, \end{aligned}$$

where equation (28) has been made use of. Setting $t = 0$, equation (37) becomes:

$$\langle \nabla_x^2 F(v), v \rangle_x = \langle \partial_x^2 F(v), v \rangle^{\mathrm{E}} - \langle \partial_x F, \Gamma_x(v, v) \rangle^{\mathrm{E}}, \ \forall v \in T_x M, \tag{38}$$

which provides an operative definition of the Riemannian Hessian operator. By solving the above equation, the Riemannian Hessian operator may be written as:

$$\nabla_x^2 F(v) = \nabla_v \nabla F = \nabla_v \mathcal{G}(x), \tag{39}$$

namely, the Riemannian Hessian of a real-valued function F at a point x on a manifold M applied to the vector v on $T_x M$ equals the covariant derivative of the Riemannian gradient vector field $\mathcal{G}$ along the direction v.

Prepared using acsauth.cls
DOI: 10.1002/acs

An operator $F_x : T_xM \to T_xM$ is positive definite if $\langle F_x(v), v\rangle_x > 0$ for all $v \in T_xM - \{0\}$. If an operator $F_x : T_xM \to T_xM$ is positive definite, then there exists a constant $m > 0$ such that

$$m\|v\|_x^2 \leq \langle F_x(v), v\rangle_x \text{ for all } v \in T_xM. \tag{40}$$

To prove such property, define the function $Q(v) \stackrel{\text{def}}{=} \langle F_x(v), v\rangle_x \|v\|_x^{-2}$. The function Q reaches its minimum value when $\nabla_v Q = 0$, namely when $F_x(v) - Q(v)v = 0$. Therefore, the minimum point of the function Q corresponds to the eigenvector of the function Q associated to the minimal eigenvalue $\underline{\lambda}$ and $\langle F_x(v), v\rangle_x \|v\|_x^{-2} \geq \underline{\lambda}$ for every $v \in T_xM - \{0\}$. As operator F_x is positive-definite, it holds that $\underline{\lambda} > 0$. As a consequence, selected any constant $0 < m \leq \underline{\lambda}$, inequality (40) holds true.

Given a smooth function $F : M \to \mathbb{R}$, any point $x^\star \in M$ such that $\nabla_{x^\star} F = 0$ is termed *critical* for the function F. A critical point $x^\star \in M$ where the Riemannian Hessian $\nabla^2_{x^\star} F$ is positive definite is a *local minimum* of the function F.

A retraction map $R : TM \to M$ is defined such that any restriction $R_x : T_xM \to M$, for $x \in M$, satisfies conditions (adapted from [28]):

- R_x is defined in some open ball $\mathbb{B}_x(0, r)$ of radius $r > 0$ about $0 \in T_xM$ and is continuously differentiable;
- It holds $R_x(0) = x$ for all $x \in M$;
- It holds $dR_x|_0(v) = v$ for all $v \in T_xM$.

A retraction $R_x(v)$ sends a tangent vector $v \in T_xM$ to a point in the manifold M that belongs to a neighborhood of $x \in M$, as illustrated in the Figure 3.

A geodesic $\gamma_{x,v}$ on a Riemannian manifold defines a retraction. In fact, take $R_x(tv) = \gamma_{x,v}(t)$. By definition of geodesic, the function $R_x(tv)$ is continuously differentiable and it holds that $R_x(0) = \gamma_{x,v}(0) = x$. Moreover, by definition of tangent map and by the self-parallel-translation property of geodesics, it holds that:

$$\frac{d}{dt} R_x(tv) = dR_x|_{tv}(v) = \dot{\gamma}_{x,v}(t) = \Gamma(\gamma_{x,v})_0^t v. \tag{41}$$

Hence, setting $t = 0$, it is found that $dR_x|_0(v) = v$. The above identity additionally tells that the tangent map associated to a retraction map chosen as a geodesic arc coincides with the parallel translation operator over the same geodesic arc from the starting point outward. The retraction associated to a geodesic arc is termed *exponential map* and is denoted as $\exp : TM \to M$. A restriction of the exponential map at the point $x \in M$ is defined by:

$$\exp_x(v) \stackrel{\text{def}}{=} \gamma_{x,v}(1). \tag{42}$$

When dealing with geodesic arcs on a manifold M, the natural question of finding whether there exists a geodesic arc that joins two arbitrary points on M arises, namely, whether there exists a

Prepared using acsauth.cls
DOI: 10.1002/acs

vector $v \in T_xM$ such that $\exp_x(v) = y$, for two given points $x, y \in M$. If such a vector $v \in T_xM$ exists, then it computes as $v = \exp_x^{-1}(y)$, where symbol $\exp_x^{-1} : M \to T_xM$ denotes the inverse of the exponential map (sometimes referred to as 'logarithmic map' or 'lifting map'). Given two manifolds M and N, a bijective map $f : M \to N$ is termed *diffeomorphism* if both $f : M \to N$ and its inverse $f^{-1} : N \to M$ are differentiable. Given a point $x \in M$, there exists an open ball $\mathbb{B}_x(0, r)$ in T_xM such that the map $\exp_x$ is a diffeomorphism of $\mathbb{B}_x(0, r)$ onto an open subset of the manifold M and the space $\exp_x(\mathbb{B}_x(0, r))$ is termed *normal neighborhood* of the point x. The maximum extent of the ball $\mathbb{B}_x(0, r)$ such that the map $\exp_x$ is a diffeomorphism of $\mathbb{B}_x(0, r)$ onto an open subset of the manifold M is termed *injectivity radius* at x and is denoted by $i_x(M)$. Set $\mathbb{U}_x \stackrel{\text{def}}{=} \exp_x(\mathbb{B}_x(0, i_x(M)))$ as the largest open subset of the manifold M such that the map $\exp_x$ is a diffeomorphism of $\mathbb{B}_x(0, r)$ onto an open subset of the manifold M. If the point y belongs to $\mathbb{U}_x$, then there exists a unique geodesic arc $t \mapsto \exp_x(t \exp_x^{-1}(y))$ that joins point y to point x.

3.3. Gradient method and Newton's method on differentiable manifolds

Although the present paper is devoted to the Newton's method on manifolds, the gradient method on manifolds is explained as well for completeness of exposition and for comparison purposes. The present paper generalizes the notion of gradient-based optimization and Newton-based optimization on geodesic arcs by the notion of retraction. As a reading about the geodesic-based gradient method and Newton's method on manifolds, readers may see [18].

Likewise in subsection 3.1, the optimization problem on a smooth manifold M may be cast as follows: Given a smooth function $F : M \to \mathbb{R}$ and an estimate $x \in M$ of a critical point (of minimum) $x^\star \in M$ of the criterion F, find a direction $v \in T_xM$ that points toward a better estimate of the actual minimum point and define a stepping method to move towards such a point along v.

Assume the base-manifold M is Riemannian with metric $\langle \cdot, \cdot \rangle_x$. In order to find a move-along direction, it pays to approximate the criterion function F by Taylor expansion truncated to the first-order term, namely:

$$\tilde{F}_x(v) \stackrel{\text{def}}{=} F(x) + \langle \nabla_x F, v \rangle_x. \tag{43}$$

The direction along which the function $\tilde{F}_x(v)$ decreases most rapidly with respect to the current estimate $F(x)$ is clearly given by:

$$v = -\nabla_x F, \tag{44}$$

as it minimizes the map $v \mapsto \|v\|_x^{-2} \langle \nabla_x F, v \rangle_x$ over $T_xM - \{0\}$.

If a second-order Taylor expansion is invoked instead, namely:

$$\bar{F}_x(v) \stackrel{\text{def}}{=} F(x) + \langle \nabla_x F, v \rangle_x + \frac{1}{2} \langle \nabla_x^2 F(v), v \rangle_x, \tag{45}$$

the move-along direction $v \in T_xM$ is the one that satisfies the analogous of condition (16), namely:

$$\nabla_v \bar{F}_x = 0. \tag{46}$$

Prepared using acsauth.cls
DOI: 10.1002/acs

Note that $\bar{F}_x : T_xM \to \mathbb{R}$, hence the vector $\nabla_v \bar{F}_x$ is a Riemannian gradient in the manifold T_xM. Identifying $T_v T_x M \cong T_x M$ and recalling that the operator $\nabla^2_x F$ is linear, it is readily found that $\nabla_v \bar{F}_x = \nabla_x F + \nabla^2_x F(v)$. The move-along direction on M is, thus:

$$v = (\nabla^2_x F)^{-1}(-\nabla_x F), \tag{47}$$

where symbol $(\nabla^2_x F)^{-1}$ denotes the inverse of the Riemannian Hessian operator which is defined upon appropriate regularity conditions on the Riemannian Hessian map $x \mapsto \nabla^2_x F$ to hold in a neighborhood of the critical point $x^\star$.

In either case, in order to move away from the initial estimate $x \in M$ along the direction $v \in T_xM$ of an extent $t > 0$, toward a new estimate $y \in M$, one may use a retraction-based stepping method expressible as:

$$y = R_x(tv). \tag{48}$$

A geodesic arc $\gamma_{x,v}$ on a Riemannian manifold M always generates a retraction $R_x(tv) = \gamma_{x,v}(t)$ but, depending on the geometry of the manifold of interest, other retractions than the exponential map might be envisaged.

In summary, optimization methods on manifolds, starting from an initial guess x_0, generate a sequence x_k, $k \in \mathbb{N} - \{0\}$, of ever refined estimates of the minimum point of a given criterion function. Two such optimization methods are:

- **Retracted Riemannian-gradient stepping method**: It is the counterpart of the gradient-steepest-descent stepping method (14) and reads:

$$x_{k+1} = R_{x_k}(-t_k \nabla_{x_k} F),\ k \in \mathbb{N}. \tag{49}$$

- **Retracted (damped) Riemannian-Newtonian stepping method**: It is the counterpart of the damped Newtonian stepping method (20) and reads:

$$x_{k+1} = R_{x_k}(-t_k (\nabla^2_{x_k} F)^{-1}(\nabla_{x_k} F)),\ k \in \mathbb{N}. \tag{50}$$

The parameter $t_k > 0$ in (49) as well as (50) denotes the optimization stepsize at step k. An optimal value of the stepsize may be chosen by adopting the counterpart of rule (12), namely:

$$t_k^\star \stackrel{\text{def}}{=} \arg\min_{t \in \mathbb{T}} \{F(R_{x_k}(t v_k))\}, \tag{51}$$

where it is understood that $v_k = -\nabla_{x_k} F$ in the case of retracted-gradient stepping or $v_k = -(\nabla^2_{x_k} F)^{-1}(\nabla_{x_k} F)$ in the case of retracted-damped-Newtonian stepping and $\mathbb{T} \subset \mathbb{R}^+$ is an appropriate interval. Section 4 deals with the well-definedness issues related to the algorithms (49) and (50) with stepsize selection rule (51).

Solving the problem (51) may result unpractical, therefore sub-optimal stepsize selection methods were devised in the optimization literature (see, for example, reference [5] for the case $M = \mathbb{R}^n$). By

Prepared using acsauth.cls
DOI: 10.1002/acs

definition of retraction, $t \mapsto R_{x_k}(tv_k)$ is a smooth curve for sufficiently small t, hence the following truncated Taylor expansion holds around $t = 0$:

$$\bar{F}(R_{x_k}(tv_k)) = F(x_k) + t\langle \nabla_{x_k} F, v_k \rangle_{x_k} + \frac{t^2}{2} \langle \nabla^2_{x_k} F(v_k), v_k \rangle_{x_k}. \tag{52}$$

A sub-optimal optimization stepsize is taken as one that minimizes the quantity $\bar{F}(R_{x_k}(tv_k))$, namely:

$$\bar{t}_k^\star \stackrel{\text{def}}{=} - \frac{\langle \nabla_{x_k} F, v_k \rangle_{x_k}}{\langle \nabla^2_{x_k} F(v_k), v_k \rangle_{x_k}}, \tag{53}$$

that is acceptable as long as $\bar{t}_k^\star \in \mathbb{T}$. In particular, for the two cases of interest in the present paper, it is possible to give an explicit expression of the sub-optimal stepsize (53). In the case of the retracted Riemannian-gradient stepping method, substituting the expression $v_k = -\nabla_{x_k} F$ into the relationship (53) yields:

$$\bar{t}_k^\star = \frac{\|\nabla_{x_k} F\|^2_{x_k}}{\langle \nabla^2_{x_k} F(\nabla_{x_k} F), \nabla_{x_k} F \rangle_{x_k}}. \tag{54}$$

Note that, if the Hessian $\nabla^2_x F$ is positive-definite, then, according to the relationship (40), there exists a constant $m > 0$ such that $\bar{t}_k^\star \leq \frac{1}{m}$. In the case of the retracted Riemannian-Newtonian stepping method, substituting the expression $v_k = -(\nabla^2_{x_k} F)^{-1}(\nabla_{x_k} F)$ into the relationship (53) yields $\bar{t}_k^\star = 1$.

The present theory has been developed under the assumption that the optimization problem is well-posed and that either an optimal stepsize search is implemented or the quadratic approximation of the criterion function does not pose any serious obstacle to the convergence of the algorithm. On a practical ground, a number of problems might arise. In general, the Hessian may be positive semidefinite in correspondence to the optimal solution or even indefinite, therefore, the Newtonian method might result ill-behaving. The known remedy is to invoke a positive-definite substitute of the Hessian. In addition, in general, a stepsize selection based on a quadratic approximation of the criterion function may lead to the divergence of a Newton-like method. A known remedy is an Armijo-type rule with "backtracking" inexact line search. Such issues are discussed in the paper [4] about unconstrained optimization and in the paper [18] with reference to optimization on manifolds.

3.4. The case of the non-unitary hypersphere for blind deconvolution purpose

The manifold of interest in the present manuscript is the non-unitary hypersphere S^{n-1}_ϱ defined as:

$$S^{n-1}_\varrho \stackrel{\text{def}}{=} \{x \in \mathbb{R}^n | x^T x = \varrho^2\}, \tag{55}$$

with $\varrho > 0$. The tangent space at $x \in S^{n-1}_\varrho$ has the structure:

$$T_x S^{n-1}_\varrho \stackrel{\text{def}}{=} \{v \in \mathbb{R}^n | v^T x = 0\}. \tag{56}$$

The canonical metric on the non-unitary hypersphere is the one induced by the Euclidean metric, namely $\langle u, v \rangle_x \stackrel{\text{def}}{=} u^T v$ for any $x \in S^{n-1}_\varrho$. The canonical metric defines the norm $\|v\| \stackrel{\text{def}}{=} \sqrt{v^T v}$ on

Prepared using acsauth.cls
DOI: 10.1002/acs

$T_x S_\varrho^{n-1}$. The corresponding Christoffel form is:

$$\Gamma_x(v,v) = -\varrho^{-2}\|v\|^2 x. \tag{57}$$

The geodesic $\gamma_{x,v}(t)$ corresponding to the chosen metric finds as:

$$\gamma_{x,v}(t) = \cos(\varrho^{-1}\|v\|t)x + \varrho\|v\|^{-1}\sin(\varrho^{-1}\|v\|t)v, \tag{58}$$

for $v \neq 0$, while $\gamma_{x,0}(t) = x$. It satisfies the geodesic equation (28) where the Christoffel form assumes the expression (57). Given two points $x_1, x_2 \in S_\varrho^{n-1}$ and a geodesic arc $\gamma_{x_1,v}(t)$ with $v \in T_{x_1} S_\varrho^{n-1}$ connecting them, namely, such that $\gamma_{x_1,v}(1) = x_2$, the geodesic distance between points x_1 and x_2 is given by $\delta(x_1, x_2) = \|v\|$. From the expression (58) of the geodesic curve on the hypersphere, it follows:

$$x_2 = \cos(\varrho^{-1}\|v\|)x_1 + \varrho\|v\|^{-1}\sin(\varrho^{-1}\|v\|)v, \tag{59}$$

therefore, by recalling that $x_1^T x_1 = 1$ and $x_1^T v = 0$, an expression for the geodesic distance is readily obtained as:

$$\delta(x_1, x_2) = \varrho \arccos\left(\frac{x_1^T x_2}{\varrho^2}\right), \tag{60}$$

where function 'arccos' denotes the inverse cosine function whose image is assumed to belong to the interval $[0,\ \pi]$.

The Riemannian gradient of a smooth function $F : S_\varrho^{n-1} \to \mathbb{R}$ at a point $x \in S_\varrho^{n-1}$ finds by the condition (36) and takes on the form:

$$\nabla_x F = (e_n - \varrho^{-2} x x^T)\partial_x F, \tag{61}$$

where symbol e_n denotes a $n \times n$ identity matrix.

The Riemannian Hessian operator associated to a smooth function $F : S_\varrho^{n-1} \to \mathbb{R}$ at a point $x \in S_\varrho^{n-1}$ applied to a vector $v \in T_x S_\varrho^{n-1}$ finds by the condition (37) with Christoffel form (57). Its expression is:

$$\nabla_x^2 F(v) = [(e_n - \varrho^{-2} x x^T)\partial_x^2 F - \varrho^{-2}(x^T \partial_x F)e_n]v. \tag{62}$$

Note that, in the present case, the Riemannian Hessian may be represented by a $n \times n$ matrix $H_x \stackrel{\text{def}}{=} (e_n - \varrho^{-2} x x^T)\partial_x^2 F - \varrho^{-2}(x^T \partial_x F)e_n$, hence its inverse may be represented by matrix H_x^{-1}.

A retraction map on the manifold S_ϱ^{n-1} is given by the geodesic formula:

$$\exp_x(v) \stackrel{\text{def}}{=} \begin{cases} \cos(\varrho^{-1}\|v\|)x + \varrho\|v\|^{-1}\sin(\varrho^{-1}\|v\|)v, & \text{for} \quad v \neq 0, \\ x, & \text{for} \quad v = 0. \end{cases} \tag{63}$$

A further retraction map is defined in terms of the projection onto the manifold S_ϱ^{n-1} (adapted from [17]):

$$R_x(v) \stackrel{\text{def}}{=} \varrho\|x + v\|^{-1}(x + v). \tag{64}$$

DOI: 10.1002/acs

Algorithm 1 Pseudocode to implement the retracted-Riemannian-Newtonian optimization method on the hypersphere S_ϱ^{n-1}.

Set x_0 to an initial guess in S_ϱ^{n-1} and K to the desired number of iterations
for $k = 0$ to K **do**
  Compute $g_k = (e_n - \varrho^{-2} x_k x_k^T)\partial_{x_k} F$
  Compute $H_k = (e_n - \varrho^{-2} x_k x_k^T)\partial_{x_k}^2 F - \varrho^{-2}(x_k^T \partial_{x_k} F)e_n$
  Set $v_k = -H_k^{-1} g_k$
  Solve for $t_k^\star = \arg\min_{t\in\mathbb{T}}\{F(R_{x_k}(tv_k))\}$
  Update $x_{k+1} = R_{x_k}(t_k v_k)$
end for

For the convenience of the reader, the retracted-Riemannian-Newtonian optimization method on the hypersphere S_ϱ^{n-1} is summarized in the Algorithm 1. Instead of a fixed number of iterations, the algorithm may halt the iteration as soon as a suitable exit condition is met. The most typical condition is that the norm of the Riemannian gradient becomes smaller than a given threshold.

For blind deconvolution purpose, the dimension of the manifold n is set to the length L_x of the impulse response of the inverse filter. As underlined in the subsection 2.3, the convolution between two real-valued sequences of finite-length n may be represented by the Euclidean inner product in $\mathbb{R}^n$. Hence, the criterion function (4) to optimize may be rewritten in vectorial form as a function of the type:

$$F(x) = \frac{1}{2}\mathfrak{E}[(x^T\bar{b} - A(x^T\bar{b}))^2], \tag{65}$$

with $x \in \mathrm{S}_\varrho^{n-1}$ representing the inverse-filter impulse response and $\bar{b} \in \mathbb{R}^n$ representing the current filter-buffer pattern. The discrete-time index drop for the ease of notation and the expectation $\mathfrak{E}$ is evaluated on the statistics of the random vector $\bar{b}$. Hence, the Euclidean gradient and the Hessian matrix of the criterion function F are computed as:

$$\partial_x F = \mathfrak{E}[(x^T\bar{b} - A(x^T\bar{b}))(1 - \dot{A}(x^T\bar{b}))\bar{b}], \tag{66}$$

$$\partial_x^2 F = \mathfrak{E}[((1 - \dot{A}(x^T\bar{b}))^2 - (x^T\bar{b} - A(x^T\bar{b}))\ddot{A}(x^T\bar{b}))\bar{b}\bar{b}^T], \tag{67}$$

respectively. (The gradient (66) appears as a weighted (or non-linear) temporal average buffer-vector of the adaptive inverse filter, while the Hessian matrix (67) appears as a non-linear correlation matrix of the input-stream of the adaptive inverse filter.) In some circumstance of interest in blind signal processing, the following approximation holds:

$$\begin{aligned}&\mathfrak{E}[((1 - \dot{A}(x^T\bar{b}))^2 - (x^T\bar{b} - A(x^T\bar{b}))\ddot{A}(x^T\bar{b}))\bar{b}\bar{b}^T]\\ &\approx \mathfrak{E}[((1 - \dot{A}(x^T\bar{b}))^2 - (x^T\bar{b} - A(x^T\bar{b}))\ddot{A}(x^T\bar{b}))]\mathfrak{E}[\bar{b}\bar{b}^T].\end{aligned} \tag{68}$$

DOI: 10.1002/acs

In the hypothesis that $\mathfrak{E}[\bar{b}] = 0$, $C_{\bar{b}\bar{b}} \stackrel{\text{def}}{=} \mathfrak{E}[\bar{b}\bar{b}^T]$ is the time-covariance of the input stream signal, and:

$$\partial_x^2 F \approx \mathfrak{E}[((1 - \dot{A}(x^T\bar{b}))^2 - (x^T\bar{b} - A(x^T\bar{b}))\ddot{A}(x^T\bar{b}))]C_{\bar{b}\bar{b}}. \tag{69}$$

As it will be mentioned in section 5.1, the above expression may be further simplified as it might be possible to assume $C_{\bar{b}\bar{b}} = e_n$.

4. CONVERGENCE RESULTS

The present subsection discusses issues related to the well-definedness, convergence and rate of convergence of the retracted-Riemannian-gradient optimization algorithm as well as of the retracted-damped-Riemannian-Newtonian algorithm. On a scale of increasing complexity, subsection 4.1 recalls the proof of quadratic convergence of the Newtonian method on the Euclidean space $\mathbb{R}^n$, subsection 4.2 discusses the convergence of the retracted-Riemannian-gradient method on manifolds and subsection 4.3 discusses the convergence properties of the retracted-Riemannian-Newtonian method on manifolds.

4.1. Convergence properties of the Newtonian method on the space $\mathbb{R}^n$

Suppose that an optimization method generates a sequence $x_k \in \mathbb{R}^n$ that converges to a point $x^\star \in \mathbb{R}^n$. The sequence is said to converge *quadratically* if there exists a constant $B > 0$ such that

$$\|x_{k+1} - x^\star\| \leq B\|x_k - x^\star\|^2, \tag{70}$$

for all k sufficiently large. Here, symbol $\|\cdot\|$ denotes the Euclidean norm in $\mathbb{R}^n$, hence, given two points $x, y \in \mathbb{R}^n$, the quantity $\|x - y\|$ denotes the Euclidean distance between $x \in \mathbb{R}^n$ and $y \in \mathbb{R}^n$. Quadratic convergence has two noticeable consequences. A first consequence is that, if the initial guess is sufficiently close to the optimal solution, the Newton's method will rapidly converge toward the optimal solution. A second consequence is that it provides a criterion to stop iteration.

In order to analyze the convergence features of the Newton method, the following definition and properties are worth recalling:

- Let $F : \mathbb{E}^n \to \mathbb{E}^m$ denote an operator. Its operator norm induced by the Euclidean norm is defined as:
$$\|F\| \stackrel{\text{def}}{=} \max_{x \in \mathbb{E}^n - \{0\}} \{\|F(x)\|\|x\|^{-1}\}. \tag{71}$$
It holds $\|F(x)\| \leq \|F\|\|x\|$ and $\|F \circ G\| \leq \|F\|\|G\|$, for all operators $F : \mathbb{E}^n \to \mathbb{E}^m$, $G : \mathbb{E}^m \to \mathbb{E}^p$ and for all $x \in \mathbb{E}^n$.
- Let $F : \mathbb{E}^n \to \mathbb{E}^m$ denote a smooth operator and let $x, y \in \mathbb{E}^n$ denote two distinct points on the Euclidean space $\mathbb{E}^n$. The curve $t \mapsto x + t(y - x)$, with $t \in [0\ 1]$, joins the points x and y

Prepared using acsauth.cls
DOI: 10.1002/acs

on the Euclidean space. The fundamental theorem of calculus ensures that:

$$F(y) - F(x) = \int_0^1 \partial_{x+t(y-x)} F(y-x) dt. \tag{72}$$

Such property follows from the following instance of the fundamental theorem of calculus:

$$F(y) - F(x) = \int_0^1 \frac{d}{dt} F(x + t(y-x)) dt. \tag{73}$$

- An operator $F : \mathbb{E}^n \to \mathbb{E}^m$ is said to be (locally) *Lipschitz continuous* on $\mathbb{S} \subset \mathbb{E}^n$ if there exists a constant $L > 0$ such that:

$$\|F(y) - F(x)\| \leq L\|y - x\| \text{ for all } x, y \in \mathbb{S}. \tag{74}$$

  Local Lipschitz continuity implies local continuity and is a weaker condition than local differentiability.

Let $F : \mathbb{R}^n \to \mathbb{R}$ be a smooth bounded-from-below function whose local minima are sought for and let $x^\star$ be one of such nondegenerate critical points of the function F (namely, $\partial_{x^\star} F = 0$ and $\partial^2_{x^\star} F$ be positive-definite). The iteration rule:

$$\begin{cases} v_k = -(\partial^2_{x_k} F)^{-1} \partial_{x_k} F, \\ t_k = \arg\min_{0<t\leq 1}\{F(x_k + t v_k)\}, \\ x_{k+1} = x_k + t_k v_k, \ k = 0, 1, 2, \ldots, \end{cases} \tag{75}$$

generates a sequence $x_k \in \mathbb{R}^n$ that converges to $x^\star$ provided the Hessian operator $\partial^2_x F$ is Lipschitz continuous in a neighborhood of the critical point $x^\star$ and the initial guess x_0 lies sufficiently close to $x^\star$. The proof of such classical result on $\mathbb{R}^n$ is instructive because it may be retraced to prove the convergence of the Newton's method on manifolds and because it provides a useful information about the convergence speed.

The application of the fundamental property (72) to the operator $\partial_x F$ on a straight path joining the current iterate x_k to the optimal solution $x^\star$ gives:

$$\partial_{x_k} F = \int_0^1 \partial^2_{x^\star + \theta(x_k - x^\star)} F(x_k - x^\star) d\theta. \tag{76}$$

A simple manipulation gives:

$$\partial_{x_k} F - \partial^2_{x^\star} F(x_k - x^\star) = \int_0^1 (\partial^2_{x^\star + \theta(x_k - x^\star)} F - \partial^2_{x^\star} F)(x_k - x^\star) d\theta. \tag{77}$$

Prepared using acsauth.cls
DOI: 10.1002/acs

By making use of the properties of integrals, the properties of the operator norm and the Lipschitz condition, it is seen that:

$$\begin{aligned}
\|\partial_{x_k} F - \partial^2_{x^\star} F(x_k - x^\star)\| &= \left\| \int_0^1 (\partial^2_{x^\star + \theta(x_k - x^\star)} F - \partial^2_{x^\star} F)(x_k - x^\star) d\theta \right\| \\
&\leq \int_0^1 \|(\partial^2_{x^\star + \theta(x_k - x^\star)} F - \partial^2_{x^\star} F)(x_k - x^\star)\| d\theta \\
&\leq \int_0^1 \|\partial^2_{x^\star + \theta(x_k - x^\star)} F - \partial^2_{x^\star} F\| \|x_k - x^\star\| d\theta \\
&\leq \int_0^1 L\|\theta(x_k - x^\star)\| \, \|x_k - x^\star\| d\theta \\
&= L\|x_k - x^\star\|^2 \int_0^1 \theta d\theta \\
&= \frac{1}{2} L \|x_k - x^\star\|^2. \qquad (78)
\end{aligned}$$

By continuity, in a neighborhood of $x^\star$ the Hessian $\partial^2_x F$ is nonsingular and there exists a constant m such as $\|(\partial^2_x F)^{-1}\| \leq \frac{1}{m}$ and a constant $\mu > 0$ such that $\|\partial^2_x F\| \leq \mu$. The iteration rule (75) may be written as:

$$\begin{aligned}
x_{k+1} - x^\star &= x_k - x^\star - t_k (\partial^2_{x_k} F)^{-1} \partial_{x_k} F \\
&= (\partial^2_{x_k} F)^{-1} \partial^2_{x_k} F (x_k - x^\star) - \\
&\quad t_k (\partial^2_{x_k} F)^{-1} [\partial_{x_k} F - \partial^2_{x^\star} F (x_k - x^\star) + \partial^2_{x^\star} F (x_k - x^\star)] \\
&= (\partial^2_{x_k} F)^{-1} (\partial^2_{x_k} F - t_k \partial^2_{x^\star} F)(x_k - x^\star) - \\
&\quad t_k (\partial^2_{x_k} F)^{-1} [\partial_{x_k} F - \partial^2_{x^\star} F (x_k - x^\star)]. \qquad (79)
\end{aligned}$$

The distance between the next iterate x_k and the optimal solution $x^\star$ may be related to the distance between the current estimate x_k and the optimal solution $x^\star$. In fact, it holds that:

$$\begin{aligned}
\|x_{k+1} - x^\star\| &\leq \|(\partial^2_{x_k} F)^{-1}\| \|\partial^2_{x_k} F - t_k \partial^2_{x^\star} F\| \|x_k - x^\star\| + \\
&\quad t_k \|\partial^2_{x_k} F\|^{-1} \|\partial_{x_k} F - \partial^2_{x^\star} F (x_k - x^\star)\|. \qquad (80)
\end{aligned}$$

Note that it holds:

$$\begin{aligned}
\|\partial^2_{x_k} F - t_k \partial^2_{x^\star} F\| &= \|\partial^2_{x_k} F - t_k \partial^2_{x_k} F + t_k \partial^2_{x_k} F - t_k \partial^2_{x^\star} F\| \\
&= \|(1 - t_k)\partial^2_{x_k} F + t_k (\partial^2_{x_k} F - \partial^2_{x^\star} F)\| \\
&\leq (1 - t_k)\mu + t_k \|\partial^2_{x_k} F - \partial^2_{x^\star} F\|. \qquad (81)
\end{aligned}$$

By using again the Lipschitz continuity of the Hessian operator in a neighborhood of the optimal solution and by recalling that the bound (78) holds, the inequality (80) may be rewritten as:

$$\begin{aligned}
\|x_{k+1} - x^\star\| &\leq \frac{1}{m}[(1 - t_k)\mu + t_k L \|x_k - x^\star\|] \|x_k - x^\star\| + \frac{L}{2m} \|x_k - x^\star\|^2 \\
&\leq (1 - t_k)\frac{\mu}{m} \|x_k - x^\star\| + t_k \frac{3L}{2m} \|x_k - x^\star\|^2. \qquad (82)
\end{aligned}$$

Prepared using acsauth.cls
DOI: 10.1002/acs

In general, the convergence speed of the damped Newtonian algorithm depends on the magnitude of the learning stepsize schedule. If the stepsize schedule is chosen as the constant value $t_k = 1$, then the Newtonian algorithm is undamped and converges quadratically.

The fundamental theorem of calculus, that relates the magnitude of the gradient of the criterion F with the magnitude of its Hessian, as well as the Lipschitz continuity of the Hessian operator, constitute the core instruments to prove the quadratic convergence of the Newton's iteration rule (75) on the Euclidean space $\mathbb{R}^n$. Clearly they will need to be extended to a general manifold to prove the convergence of a retracted-Newtonian method.

4.2. Convergence properties of the retracted-Riemannian-gradient method

Gradient descent algorithms on manifolds share the well-characterized convergence properties of their analog in Euclidean spaces. Such algorithms converge linearly to a local minimum of the criterion function that depends on the initial condition. The present analysis extends the convergence analysis of the Riemannian-gradient-based methods on geodesic arcs carried out in [18]. Let M denote a Riemannian manifold and $F : M \to \mathbb{R}$ a bounded-from-below criterion function whose local minima are sought for. Let $x^\star \in M$ denote a nondegenerate critical point (of minimum) of the criterion F. The retracted-Riemannian-gradient rule writes:

$$\begin{cases} v_k = -\nabla_{x_k} F, \\ t_k = \arg\min_{t>0}\{F(R_{x_k}(tv_k)) \,|\, tv_k \in \mathbb{B}_{x_k}(0,r)\}, \\ x_{k+1} = R_{x_k}(t_k v_k),\ k = 0, 1, 2, \ldots, \end{cases} \tag{83}$$

with $R : TM \to M$ being a retraction map such that every restriction R_x is defined within an open ball $\mathbb{B}_x(0,r) \subset T_x M$ with $r > 0$.

Define $\mathbb{W}_k$ as the connected component of the level set $\{x \in M \,|\, F(x) \leq F(x_k)\}$ which contains x_k. If the criterion function $F : M \to \mathbb{R}$ is continuously differentiable with continuous gradient field $\nabla_x F$, the set $\mathbb{W}_0$ is compact and the map $dR_x|_v$ is continuous for every $x \in \mathbb{W}_0$ and $v \in \mathbb{B}_x(0,r)$, the sequence generated by the retracted-Riemannian-gradient algorithm (83) converges to a critical point $x^\star \in \mathbb{W}_0$ of the criterion function, provided the critical values of the criterion function F are distinct.

The convergence of the retracted-Riemannian-gradient algorithm (83) may be illustrated by adapting the proof discussed in [18].

Suppose that the current iterate x_k is not a critical point. For the ease of notation, define:

$$J_k(t) \stackrel{\text{def}}{=} F(R_{x_k}(-t\nabla_{x_k} F)). \tag{84}$$

Note that $J_k(0) = F(x_k)$. In addition, define:

$$\mathbb{J}_k \stackrel{\text{def}}{=} \{t > 0 \,|\, t\nabla_{x_k} F \in \mathbb{B}_{x_k}(0,r) \text{ and } J_k(t) < J_k(0)\}, \tag{85}$$

$$\bar{t}_k \stackrel{\text{def}}{=} \limsup \mathbb{J}_k. \tag{86}$$

Prepared using acsauth.cls
DOI: 10.1002/acs

The set $\mathbb{J}_k$ contains all the feasible values of the learning stepsize at iteration k, namely, all the values of the parameter t that correspond to a decrease of the criterion function F with respect to the current value $F(x_k)$. Note that it holds:

$$\dot{J}_k(t) = \langle \nabla_{R_{x_k}(-t\nabla_{x_k}F)}F, dR_{x_k}|_{-t\nabla_{x_k}F}(-\nabla_{x_k}F)\rangle_{R_{x_k}(-t\nabla_{x_k}F)}, \tag{87}$$

hence:

$$\dot{J}_k(0) = \langle \nabla_{x_k}F, -\nabla_{x_k}F\rangle_{x_k} = -\|\nabla_{x_k}F\|^2_{x_k} < 0, \tag{88}$$

therefore the set $\mathbb{J}_k$ is not empty. The quantity $\bar{t}_k$ denotes the maximum admissible value of the learning stepsize at iteration k. Therefore, the stepsize t_k in (83) is well-defined and $0 < t_k < \bar{t}_k$.

As t_k is a critical point of the function $J_k(t)$, it holds $\dot{J}_k(t_k) = 0$. Choose a constant $\alpha_k \in (0\ \frac{1}{2})$. As the function $\dot{J}_k$ given by equation (87) is continuous in $[0\ t_k]$, the equation $\dot{J}_k(t) = \alpha_k \dot{J}_k(0)$ admits a *smallest* solution $\hat{t}_k \in (0\ t_k)$ and it holds:

$$\dot{J}_k(t) < \alpha_k \dot{J}_k(0) \text{ for all } t \in [0\ \hat{t}_k). \tag{89}$$

The variation of the function F from the current iterate to the next iterate may be evaluated as:

$$F(x_{k+1}) - F(x_k) = J_k(t_k) - J_k(0) < J_k(\hat{t}_k) - J_k(0). \tag{90}$$

The fundamental theorem of calculus applied to the function $J_k(t)$ reads:

$$J_k(\hat{t}_k) - J_k(0) = \int_0^1 \dot{J}_k(\theta\hat{t}_k)\hat{t}_k d\theta. \tag{91}$$

In conjunction with the inequality (89), it leads to the estimation:

$$J_k(\hat{t}_k) - J_k(0) \leq \hat{t}_k(\alpha_k \dot{J}_k(0)). \tag{92}$$

Hence, because of the identity (88), the conclusion below follows:

$$F(x_{k+1}) - F(x_k) < -\alpha_k \hat{t}_k \|\nabla_{x_k}F\|^2_{x_k}. \tag{93}$$

The sequence $F(x_k)$ is monotone decreasing. As the critical points of F are distinct, the sequence x_k converges to one of these critical points.

4.3. Convergence properties of the retracted-Riemannian-Newtonian method

The present analysis extends the study of the convergence properties of the Riemannian-Newtonian methods on geodesics carried out in [18, 32] and retraces the analysis illustrated in the subsection 4.1. In the context of optimization methods on Riemannian manifolds, the sequence $x_k \in M$ generated by an optimization algorithm is said to converge *quadratically* to a critical point $x^\star \in M$ if there exists a constant $B > 0$ such that

$$\delta(x_{k+1}, x^\star) \leq B\delta^2(x_k, x^\star), \tag{94}$$

DOI: 10.1002/acs

for all k sufficiently large, where $\delta : M \times M \to \mathbb{R}_0^+$ denotes geodesic distance.

Let M denote a Riemannian manifold and $F : M \to \mathbb{R}$ a bounded-from-below criterion function whose local minima are sought for. The retracted-Riemannian-Newtonian rule writes:

$$\begin{cases} v_k = -(\nabla^2_{x_k} F)^{-1}(\nabla_{x_k} F), \\ t_k = \arg\min_{0<t\leq 1}\{F(R_{x_k}(tv_k)) \,|\, tv_k \in \mathbb{B}_{x_k}(0,r)\}, \\ x_{k+1} = R_{x_k}(t_k v_k),\ k = 0, 1, 2, \ldots, \end{cases} \tag{95}$$

with $R : TM \to M$ being a retraction map defined on open balls $\mathbb{B}_\cdot(0,r)$.

In order to analyze the convergence features of the Newton's method on manifolds, the following definitions and properties are worth recalling:

- Let $x \in M$ and let $F_x : T_x M \to T_x M$ be an operator. Its operator norm is defined as:

$$\|F_x\|_x \stackrel{\text{def}}{=} \max_{v \in T_x M - \{0\}} \{\|F_x(v)\|_x \|v\|_x^{-1}\}. \tag{96}$$

- Let $c : [0\ 1] \to M$ denote a smooth curve on the Riemannian manifold M endowed with a parallel translation operator $\Gamma(c)$ on the curve c and $\mathcal{V} \in \mathfrak{X}(M)$ denote a vector field on M. Let $x \stackrel{\text{def}}{=} c(0)$ and $y \stackrel{\text{def}}{=} c(1)$. The fundamental theorem of calculus for vector fields may be written:

$$\Gamma(c)_1^0 \mathcal{V}(y) = \mathcal{V}(x) + \int_0^1 \Gamma(c)_\theta^0 \nabla_{\dot{c}(\theta)} \mathcal{V} d\theta, \tag{97}$$

  as may be proven by using the identity

$$\int_0^1 \frac{d}{d\theta} \Gamma(c)_\theta^0 \mathcal{V}(c(\theta)) d\theta = \Gamma(c)_1^0 \mathcal{V}(c(1)) - \Gamma(c)_0^0 \mathcal{V}(c(0)) = \Gamma(c)_1^0 \mathcal{V}(y) - \mathcal{V}(x) \tag{98}$$

  together with the identity (24). Given a continuously differentiable function $F : M \to \mathbb{R}$, the fundamental theorem of calculus applied to the gradient vector field of F gives:

$$\Gamma(c)_1^0 \nabla_y F = \nabla_x F + \int_0^1 \Gamma(c)_\theta^0 \nabla^2_{\dot{c}(\theta)} F(\dot{c}(\theta)) d\theta. \tag{99}$$

- Let M be a Riemannian manifold, $F : M \to \mathbb{R}$ a twice differentiable function and $R : TM \to M$. Given a point $x \in M$ and a domain $\mathbb{B}_x(0,r) \ni v$ where R_x is defined and denoted as $\Gamma(R_x(tv))$: the parallel translation operation along the curve $R_x(tv)$, the Riemannian Hessian operator $\nabla^2_x F$ is locally Lipschitz continuous (at $v = 0$) over the curve $[0\ 1] \ni t \mapsto R_x(tv)$ on a subset $\mathbb{S} \subset M$, if there exists a constant $L > 0$ such that:

$$\|\Gamma(R_x(tv))_1^0 \circ \nabla^2_{R_x(v)} F \circ dR_x|_v - \nabla^2_x F\|_x \leq L\|v\|_x \tag{100}$$

  for any $x \in \mathbb{S}$ and any $v \in \mathbb{B}_x(0,r)$. Note that if $M = \mathbb{R}^n$ endowed with the standard Euclidean inner product, then $R_x(tv) = x + tv$, $dR_x|_{tv}(v) = v$ and $\Gamma(R_x(tv))_1^0(w) = w$ for any $x, v, w \in \mathbb{R}^n$, hence condition (100) collapses into condition (74) applied to the operator $\partial^2_x F$.

DOI: 10.1002/acs

Let $x^\star$ denote a non-degenerate critical point of the function F and $\nabla^2_{x^\star}F$ be positive definite. Let $R : TM \to M$ denote a retraction with existence domains $\mathbb{B}_x(0,r)$. If the Riemannian Hessian operator $\nabla^2_x F$ is Lipschitz continuous over the curve $t \mapsto R_x(tv)$ and continuous in a neighborhood of the critical point $x^\star$ and the initial point x_0 of the iteration (95) is sufficiently close to the critical point $x^\star$ then the iteration (95) converges to $x^\star$.

Suppose that the current iterate x_k is not a critical point and define the auxiliary function $J_k(t) \stackrel{\text{def}}{=} F(R_{x_k}(tv_k))$. By the chain rule of derivatives, it is found that $\dot{J}_k(t) = \langle \nabla_{R_{x_k}(tv_k)}F, dR_{x_k}|_{tv_k}(v_k)\rangle_{R_{x_k}(tv_k)}$. In particular, it holds $\dot{J}_k(0) = -\langle \nabla_{x_k}F, (\nabla^2_{x_k}F)^{-1}(\nabla_{x_k}F)\rangle_x$. By continuity, in a neighborhood of the critical point $x^\star$, the Riemannian Hessian $\nabla^2_x F$ is positive definite and hence its inverse is positive definite as well. Therefore, $\dot{J}_k(0) < 0$ and the optimal stepsize schedule (95) is well defined.

Because of the positive-definiteness and continuity of the Riemannian Hessian operator $\nabla^2_{x^\star}F$, there exist constants $m, \mu > 0$ such that $\|\nabla^2_x F\|_x \leq \mu$ and $m\|v\|^2_x \leq \langle \nabla^2_x F(v), v\rangle_x$ for every $v \in T_xM$, in a neighborhood of the critical point $x^\star$. Note that this also implies $\|(\nabla^2_x F)^{-1}\|_x \leq \frac{1}{m}$.

Assume that the succession x_k belongs to a normal neighborhood of the critical point $x^\star$. Let $\gamma_{x_k,q_k} : [0\ 1] \to M$ denote the geodesic arc connecting the iterate $x_k \in M$, as initial point of the arc, and the critical point $x^\star \in M$. The fundamental theorem of calculus for vector fields applied to the gradient vector field ∇F over the curve γ_{x_k,q_k} allows writing:

$$\Gamma(\gamma_{x_k,q_k})_1^0 \nabla_{x^\star}F = \nabla_{x_k}F + \int_0^1 \Gamma(\gamma_{x_k,q_k})_\theta^0 \circ \nabla^2_{\gamma_{x_k,q_k}(\theta)}F \circ \Gamma(\gamma_{x_k,q_k})_0^\theta(q_k)d\theta. \tag{101}$$

As $\nabla_{x^\star}F = 0$, using twice the self-parallel-translation property of geodesic arcs, the metric property of parallel translation and the definition of geodesic distance, yields:

$$\begin{aligned}
&-\langle \nabla_{x_{k+1}}F, q_{k+1}\rangle_{x_{k+1}} \\
&\quad = \int_0^1 \langle \Gamma(\gamma_{x_{k+1},q_{k+1}})_\theta^0 \nabla^2_{\gamma_{x_{k+1},q_{k+1}}(\theta)}F(\dot{\gamma}_{x_{k+1},q_{k+1}}(\theta)), q_{k+1}\rangle_{x_{k+1}}d\theta \\
&\quad = \int_0^1 \langle \nabla^2_{\gamma_{x_{k+1},q_{k+1}}(\theta)}F(\dot{\gamma}_{x_{k+1},q_{k+1}}(\theta)), \dot{\gamma}_{x_{k+1},q_{k+1}}(\theta)\rangle_{\gamma_{x_{k+1},q_{k+1}}(\theta)}d\theta \\
&\quad \geq m\int_0^1 \|\dot{\gamma}_{x_{k+1},q_{k+1}}(\theta)\|^2_{\gamma_{x_{k+1},q_{k+1}}(\theta)}d\theta = m\delta^2(x_{k+1},x^\star).
\end{aligned} \tag{102}$$

From the Cauchy-Schwarz inequality on $T_{x_{k+1}}M$, it is found that $m\delta^2(x_{k+1},x^\star) \leq -\langle \nabla_{x_{k+1}}F, q_{k+1}\rangle_{x_{k+1}} \leq \|\nabla_{x_{k+1}}F\|_{x_{k+1}}\|q_{k+1}\|_{x_{k+1}} = \|\nabla_{x_{k+1}}F\|_{x_{k+1}}\delta(x_{k+1},x^\star)$. In conclusion:

$$m\delta(x_{k+1},x^\star) \leq \|\nabla_{x_{k+1}}F\|_{x_{k+1}}. \tag{103}$$

Moreover, from equation (101), it follows that:

$$\begin{aligned}
\|\nabla_{x_k}F\|_{x_k} &\leq \int_0^1 \|\Gamma(\gamma_{x_k,q_k})_\theta^0 \circ \nabla^2_{\gamma_{x_k,q_k}(\theta)}F \circ \Gamma(\gamma_{x_k,q_k})_0^\theta(q_k)\|_{x_k}d\theta \\
&\leq \|q_k\|_{x_k}\int_0^1 \|\nabla^2_{\gamma_{x_k,q_k}(\theta)}F\|_{\gamma_{x_k,q_k}(\theta)}d\theta \leq \mu\|q_k\|_{x_k},
\end{aligned} \tag{104}$$

Prepared using acsauth.cls
DOI: 10.1002/acs

namely:

$$\|\nabla_{x_k} F\|_{x_k} \leq \mu \delta(x_k, x^\star). \tag{105}$$

From the fundamental theorem of calculus for vector fields applied to the Riemannian gradient vector field and to the curve $[0\ t_k] \ni t \mapsto R_{x_k}(tv_k)$, with initial velocity v_k chosen as in (95), it follows:

$$\Gamma(R_{x_k}(tv_k))_{t_k}^0 \nabla_{x_{k+1}} F = \nabla_{x_k} F + \int_0^{t_k} \Gamma(R_{x_k}(tv_k))_\theta^0 \circ \nabla^2_{R_{x_k}(\theta v_k)} F \circ dR_{x_k}|_{\theta v_k}(v_k) d\theta. \tag{106}$$

Since $v_k = -(\nabla^2_{x_k} F)^{-1}(\nabla_{x_k} F)$, it holds $\nabla_{x_k} F + \nabla^2_{x_k} F(v_k) = 0$. Plugging such a relationship into the identity (106) leads to the equation:

$$\Gamma(R_{x_k}(tv_k))_{t_k}^0 \nabla_{x_{k+1}} F = \frac{1}{t_k} \int_0^{t_k} [t_k \Gamma(R_{x_k}(tv_k))_\theta^0 \circ \nabla^2_{R_{x_k}(\theta v_k)} F \circ dR_{x_k}|_{\theta v_k} - \nabla^2_{x_k} F](v_k) d\theta. \tag{107}$$

As the parallel translation is metric and the Riemannian Hessian of the criterion function is locally Lipschitzian with Lipschitz constant L over the retraction-based curve connecting the current iterate to the next iterate, it results:

$$\|\nabla_{x_{k+1}} F\|_{x_{k+1}} \leq \frac{\|v_k\|_{x_k}}{t_k} \int_0^{t_k} \|t_k \Gamma(R_{x_k}(tv_k))_\theta^0 \circ \nabla^2_{R_{x_k}(\theta v_k)} F \circ dR_{x_k}|_{\theta v_k} - \nabla^2_{x_k} F\|_{x_k} d\theta. \tag{108}$$

Note that it holds that:

$$\begin{aligned}
&\|t_k \Gamma(R_{x_k}(tv_k))_\theta^0 \circ \nabla^2_{R_{x_k}(\theta v_k)} F \circ dR_{x_k}|_{\theta v_k} - \nabla^2_{x_k} F\|_{x_k} = \\
&\|t_k \Gamma(R_{x_k}(tv_k))_\theta^0 \circ \nabla^2_{R_{x_k}(\theta v_k)} F \circ dR_{x_k}|_{\theta v_k} - \nabla^2_{x_k} F + t_k \nabla^2_{x_k} F - t_k \nabla^2_{x_k} F\|_{x_k} = \\
&\|t_k [\Gamma(R_{x_k}(tv_k))_\theta^0 \circ \nabla^2_{R_{x_k}(\theta v_k)} F \circ dR_{x_k}|_{\theta v_k} - \nabla^2_{x_k} F] - (1 - t_k) \nabla^2_{x_k} F\|_{x_k} \leq \\
&t_k \|\Gamma(R_{x_k}(tv_k))_\theta^0 \circ \nabla^2_{R_{x_k}(\theta v_k)} F \circ dR_{x_k}|_{\theta v_k} - \nabla^2_{x_k} F\|_{x_k} + (1 - t_k) \|\nabla^2_{x_k} F\|_{x_k} \leq \\
&t_k L \|\theta v_k\|_{x_k} + (1 - t_k)\mu,
\end{aligned} \tag{109}$$

where the last inequality was obtained by invoking the Lipschitz condition and the bound on the Hessian. Plugging such inequality into the relationship (108) yields:

$$\|\nabla_{x_{k+1}} F\|_{x_{k+1}} \leq \frac{\|v_k\|_{x_k}}{t_k} \int_0^{t_k} [t_k L \|\theta v_k\|_{x_k} + (1 - t_k)\mu] d\theta = \|v_k\|_{x_k} \left[L \|v_k\|_{x_k} \frac{t_k^2}{2} + (1 - t_k)\mu \right]. \tag{110}$$

For better clarity, the quantities used in the above equations are depicted in the Figure 4. Note that $\|v_k\|_{x_k} \leq \|(\nabla^2_{x_k} F)^{-1}\|_{x_k} \|\nabla_{x_k} F\|_{x_k} \leq \frac{1}{m} \|\nabla_{x_k} F\|_{x_k}$, hence:

$$\|\nabla_{x_{k+1}} F\|_{x_{k+1}} \leq \frac{L t_k^2}{2m^2} \|\nabla_{x_k} F\|^2_{x_k} + (1 - t_k) \frac{\mu}{m} \|\nabla_{x_k} F\|_{x_k}. \tag{111}$$

Chaining together inequalities (103), (111) and (105) gives:

$$m \delta(x_{k+1}, x^\star) \leq \|\nabla_{x_{k+1}} F\|_{x_{k+1}} \leq \frac{L \mu^2 t_k^2}{2m^2} \delta^2(x_k, x^\star) + (1 - t_k) \frac{\mu^2}{m} \delta(x_k, x^\star), \tag{112}$$

Prepared using acsauth.cls
DOI: 10.1002/acs

hence:

$$\delta(x_{k+1}, x^\star) \leq \frac{L\mu^2 t_k^2}{2m^3}\delta^2(x_k, x^\star) + (1 - t_k)\frac{\mu^2}{m^2}\delta(x_k, x^\star). \quad (113)$$

The damped retracted-Riemannian-Newtonian algorithm (95) converges to the critical point $x^\star$, while the undamped algorithm (i.e., with $t_k = 1$) would converge quadratically.

5. NUMERICAL TESTS

The present section aims at illustrating the numerical behavior of the algorithms discussed in sections 3 and 4. In the following subsections, results of numerical experiments are illustrated and commented. The numerical experiments, whose implementation details are explained in the subsection 5.1, are performed on a real-world sampled telephonic channel in the noiseless-channel case as well as in the noisy-channel case, as shown in the subsection 5.2. A comparison of the deconvolution ability of the proposed algorithm and of related algorithms known from blind-deconvolution literature is presented and discussed in the subsection 5.3.

5.1. Implementation details

While the source stream s_τ is IID, after passing through the system (1), the samples of the channel output signal are no longer temporally statistically independent and, in particular, they gain second-order statistical correlation. Second order correlation is easy to remove by temporal data pre-whitening. This is not a necessary operation but it makes the deconvolution process easier. Temporal pre-whitening of a zero-mean inverse-filter input stream may be implemented by computing the covariance matrix $C_{\bar{b}\bar{b}}$ of deconvolving filter-input vector stream and by defining the whitened input vector-stream as $\hat{\bar{b}}_\tau \stackrel{\text{def}}{=} \sqrt{C_{\bar{b}\bar{b}}^{-1}}\bar{b}_\tau$. Also, as the covariance matrix is symmetric, its square root and inverse may be efficiently computed through eigenvalue decomposition achievable by efficient linear-algebra packages [19].

The above considerations give rise to the following batch-type algorithm:

- Collect the filter-input stream and form the multivariate stream $\bar{b}_\tau$.
- Whiten the multivariate stream $\bar{b}_\tau$. This operation further simplifies the expression (69) as explained in the subsection 3.4.
- Choose an initial inverse filter impulse response and iterate by the retracted-Riemannian-Newtonian algorithm applied to the whitened input stream.

In the experiments, the constant value $\varrho = 1$ was selected for the geodesic-based learning algorithms, while the constant value $\varrho = \frac{1}{2}$ was selected for the retraction-based learning algorithms. In all the following experiments, it is assumed that the source signal s_τ is a white random signal uniformly distributed within $[-\sqrt{3}, +\sqrt{3}]$. In presence of a uniformly-distributed source stream, the

DOI: 10.1002/acs

approximate Bayesian estimator

$$A(z) \stackrel{\text{def}}{=} A_1 \tanh(A_2 z) \tag{114}$$

may be used, where constants A_1 and A_2 are optimized as explained in the contributions [14, 15]. A possible difficulty when dealing with Bussgang strategies is the non-convexity of the cost function, that is the case here because the estimator A is nonlinear. The non-convexity of the cost function challenges the Newton algorithm since it only finds a local critical point. The sensitivity of the results to the initialization of the algorithm will be analyzed by numerical experiments.

The system deconvolution accuracy may be measured by means of the residual inter-symbol interference (ISI, [30]):

$$\text{ISI}_k \stackrel{\text{def}}{=} \frac{\sum_\tau T_{k,\tau}^2 - T_{k,\max}^2}{T_{k,\max}^2}\,, \tag{115}$$

where $T_{k,\tau}$ denotes the convolution between the system's impulse response and the inverse-filter's impulse response at step k and $T_{k,\max} \stackrel{\text{def}}{=} \max_\tau\{|T_{k,\tau}|\}$ denotes the maximal absolute value of the sequence $T_{k,\tau}$ at adaptation step k. The rationale of such definition is that, when the impulse response $x_{k,\tau}$ 'cancels' the channel's impulse response h_τ, the global impulse response $T_{k,\tau}$ should exhibit only one coefficient different from zero but in a real-world setting, some residual interference should be tolerated.

It was observed that the ISI measure does not properly account for the effects of channel additive noise $\mathcal{N}_\tau$, thus the quality of source signal estimate should also be measured by the mean-squared estimation error defined as:

$$\text{MSE}_k \stackrel{\text{def}}{=} \mathfrak{E}_\tau[(\zeta_{k,\tau} - s_{\tau-\Delta_k})^2], \tag{116}$$

$$\text{where } \zeta_{k,\tau} \stackrel{\text{def}}{=} \frac{z_{k,\tau}}{\sqrt{\mathfrak{E}_\tau[z_{k,\tau}^2]}}. \tag{117}$$

As it is assumed that the source signal has unit power, the inverse-filter output signal is normalized to unit-power through definition (117) before getting compared with the source signal in definition (116). The total group-delay Δ_k may be estimated as the largest lag corresponding to the sample(s) of the sequence $T_{k,\tau}$ displaying the maximal absolute value, namely, within the present paper the following definition is adopted: $\Delta_k \stackrel{\text{def}}{=} \text{largest index}\max_\tau\{|T_{k,\tau}|\}$. Also, in order to carry out experiments on noisy channels, it is worth defining the signal-to-noise ratio (SNR) as:

$$\text{SNR} \stackrel{\text{def}}{=} \frac{\mathfrak{E}_\tau[s_\tau^2]}{\mathfrak{E}_\tau[\mathcal{N}_\tau^2]}. \tag{118}$$

As the source-signal's power was assumed equal to 1, it holds that:

$$\text{SNR}_{\text{dB}} = -10\log_{10}(\mathfrak{E}_\tau[\mathcal{N}_\tau^2]). \tag{119}$$

The number of adaptation cycles is denoted as K, hence, the quantities $x_{K,\tau}$ and $T_{K,\tau}$ denote the inverse-filter impulse response and the system-filter cascade impulse response, respectively, at the end of adaptation cycles.

DOI: 10.1002/acs

The discussed algorithms have been tested to adapt an inverse filter to cancel the effects of the sampled (BGR) telephonic channel described in [2] having $L_h = 14$. The length of the inverse filter impulse response was set to $L_x = 14$ as the result of validation [13].

In the following subsections, the term 'geodesic-based Riemannian-Newtonian algorithm' denotes the Riemannian-Newtonian algorithm (50) with stepsize rule (53) where stepping-forward is implemented through the geodesic-based retraction (63), the term 'retraction-based Riemannian-Newtonian algorithm' denotes the Riemannian-Newtonian algorithm (50) with stepsize rule (53) where stepping-forward is implemented through the retraction map (64), while the term 'geodesic-based Riemannian-gradient algorithm' denotes the steepest-Riemannian-gradient-descent algorithm (49) with stepsize rule (53) where stepping-forward is implemented through the geodesic-based retraction (63).

5.2. Experiments with a noiseless and a noisy channel

A first set of results concerns the analysis of the behavior of the geodesic-based and retraction-based Riemannian-Newtonian algorithms on a noiseless channel (i.e., model (1) with $\mathcal{N}_\tau \equiv 0$ identically). About the geodesic-based Riemannian-Newtonian algorithm, the Figure 5 shows the values of the performance indices ISI and MSE, the inverse filter after $K = 50$ adaptation cycles as well as the convolution sequence $T_{k,\tau}$ after adaptation. The initial impulse response of the filter, $x_{0,\tau}$, was assumed as a null sequence, except for the 7^{th} tap-weight that was set to ϱ. The retraction-based Riemannian-Newtonian algorithm behaves in a similar way. As it is readily appreciated, in both cases the algorithm converges steadily and keeps stable after adaptation. In order to illustrate the rate of convergence of the geodesic-based Riemannian-Newtonian algorithm, the geodesic distance $\delta(x_k, x^\star)$ may be monitored during adaptation. As the optimal value of the filter-tap coefficient-vector $x^\star$ is unknown, it was assumed that $x^\star \approx x_K$ and the geodesic distances were measured after completing the cycle of iterations. The Figure 6 shows the course of the distance-sequence $k \mapsto \delta(x_k, x^\star)$ expressed as:

$$10 \log_{10} \frac{\delta(x_k, x_K)}{\delta(x_0, x_K)}.$$

A second set of results concerns the analysis of the behavior of the geodesic-based and retraction-based Riemannian-Newtonian blind-deconvolution algorithms on a noisy BGR channel for four different values of the SNR, namely 20 dB, 10 dB, 5 dB and 1 dB. In this experiment, the total number of learning iterations was set to $K = 50$. The initial impulse response of the filter was set as before. Figure 7 illustrates the behavior of the geodesic-based Riemannian-Newtonian algorithm while the Figure 8 illustrates the behavior of the retraction-based Riemannian-Newtonian algorithm. It is to be noted that, in the noisy-channel case, the geodesic-based Riemannian-Newtonian algorithm exhibits better deconvolution ability over the retraction-based Riemannian-Newtonian algorithm as the performance curves of the geodesic-based Riemannian-Newtonian algorithm

Prepared using acsauth.cls
DOI: 10.1002/acs

reach lower ISI values in correspondence of higher SNR values. However, the retraction-based Riemannian-Newtonian algorithm converges steadier and looks more stable and less influenced by the additive channel disturbance.

In order to test the dependence of the optimization ability of the optimization algorithm from the initial point, the initial point of the previous experiments was perturbed randomly on the unit hypersphere. The number of adaptation cycles was set to $K = 20$ and the noise level was set to $\mathrm{SNR} = 20$dB. Figure 9 illustrates the behavior of the projection-based Riemannian-Newtonian algorithm over 500 independent trials. The statistical analysis confirms that the algorithm reaches poor ISI levels in a small fraction of cases. It is to be underline that when the initial point is chosen as purely 'spiky' sequence (namely, a null sequence, except for the 7^{th} tap-weight that was set to ϱ) the algorithm is convergent.

5.3. Comparative numerical analysis

The presented algorithms may be compared in terms of deconvolution performances (final ISI and MSE) as well as in terms of computational complexity, with other blind deconvolution algorithms know from literature, where the elapsed-runtime is retained as a measure of the computational burden of each algorithm.

The proposed algorithms as well as six algorithms known in the literature were run on a noisy BGR telephonic channel and adapted through $K = 20$ adaptation cycles. The noise level was selected so that $\mathrm{SNR} = 20$dB. The considered algorithms for comparison purpose were the geodesic-Riemannian-Newtonian, geodesic-Riemannian-gradient, retracted-Newtonian used to optimize a Bussgang criterion function, together with five algorithms of the Bussgang family [13], namely, the Bussgang, enhanced Bussgang, Bussgang with natural gradient, enhanced Bussgang with natural gradient, fixed-point enhanced Bussgang algorithms, along with the Quasi-Maximum-Likelihood fast Newton relative optimization algorithm for blind deconvolution [4] that is relevant to the present comparison because it is based on a Newton-type optimization kernel. It is to be underlined that the relative-optimization method is based on an unconstrained optimization problem, which poses several challenges such as the possible singularity of the Hessian at some point and the need to search for an optimal stepsize via Armijo rule. The details are discussed within the paper [4] that also gives pointers to appropriate sources about how to address such numerical issues.

The results of the performed comparative analysis are summarized in the Figure 10. The performed comparative analysis shows that the retraction-based Riemannian-Newtonian algorithm exhibits the best performance among the considered non-Newton-type algorithms, thanks to the ability of the Newton algorithm to overcome the optimization ability of first-order methods. The retraction-based Riemannian-Newtonian algorithm exhibits comparable deconvolution performances with the Quasi-Maximum-Likelihood fast Newton relative optimization algorithm,

Prepared using acsauth.cls
DOI: 10.1002/acs

albeit resulting lighter from a computation burden viewpoint and easier to implement. A further comparative analysis concerns the convergence rate of the algorithms under analysis. The Figure 11 shows the result of a single run obtained with the geodesic-Riemannian-Newtonian algorithm, the retraction-Riemannian-Newtonian algorithm, the fixed-point enhanced Bussgang algorithm and the Quasi-Maximum-Likelihood fast Newton relative optimization algorithm for blind deconvolution, that exhibit the best performances. From the Figure 11 it emerges, in particular, that the retraction-Riemannian-Newtonian algorithm and the Quasi-Maximum-Likelihood fast Newton relative optimization algorithm converge with the same speed. Near convergence, the Quasi-Maximum-Likelihood fast Newton relative optimization algorithm seems to converge speedier.

6. CONCLUSION

In the recent years there has been an increasing interest in the development of efficient optimization algorithms that insist on Riemannian manifolds, with applications in statistical analysis, signal processing, machine learning as well as computer vision. Such algorithms result from the combination of insights from differential geometry, optimization and numerical analysis. The present paper provides an introduction to this rich field of applied mathematics, motivated by a specific application in signal processing. The present paper summarizes those notions of differential geometry instrumental to algorithmic development and illustrates why differential geometry provides a natural foundation for the development of numerical algorithms on manifolds. Known optimization techniques, such as steepest descent and Newton-type methods, may be generalized to the manifold setting building upon the geometric material. The constructions and computations that turn these geometrically-formulated methods into concrete numerical algorithms are explicitly given for the benefit of the readers.

In particular, the present paper introduces a class of retracted-Riemannian-Newtonian algorithms to optimize smooth criterion functions, with application to blind deconvolution. The criterion function to optimize is a Bussgang cost function of the parameters of an inverse filter whose geometrical structure is induced by an automatic-gain-control constraint. As the parameter space is a differentiable manifold, the introduced Newtonian optimization method is formulated in terms of differential-geometrical concepts and implemented according to the paradigms of numerical geometrical integration. The present paper also discusses convergence issues related to the introduced retracted-Riemannian-Newtonian optimization algorithms by extending results known for the geodesic-Riemannian-Newtonian optimization algorithms, and illustrates their performance on a comparative basis.

Prepared using acsauth.cls
DOI: 10.1002/acs

Numerical experiments show that, in the noisy-channel case, the geodesic-based Riemannian-Newtonian algorithm exhibits better deconvolution ability over the retraction-based Riemannian-Newtonian. However, the retraction-based algorithm converges steadier and looks more stable and less influenced by the additive channel disturbance. A comparative analysis that takes into account the deconvolution ability of the algorithms as well as their computational burden reveals that the retraction-based Riemannian-Newtonian algorithm exhibits the best trade-off between the optimization ability and computational complexity, among the considered algorithms.

7. ACKNOWLEDGEMENTS

The author wishes to thank the anonymous referees for a number of suggestions that helped improve the clarity of the presentation and the thoroughness of the numerical tests. The author also wishes to thank Michael Zibulevsky for sharing the computer code to implement the Quasi-Maximum Likelihood (QML) fast relative Newton algorithm.

REFERENCES

1. S. BELLINI, *Blind equalization*, Alta Frequenza, Vol. 57, pp. 445 – 450, 1988
2. A. BENVENISTE, M. GOURSAT AND G. RUGET, *Robust identification of a nonminimum phase system: Blind adjustment of a linear equalizer in data communication*, IEEE Transactions on Automatic Control, Vol. AC-25, No. 3, pp. 385 – 399, June 1980
3. D.P. BERTSEKAS AND E.M. GAFNI, *Projected Newton methods and optimization of multicommodity flows*, IEEE Transactions on Automatic Control, Vol. 28, No. 12, pp. 1090 – 1096, December 1983
4. A.M. BRONSTEIN, M.M. BRONSTEIN AND M. ZIBULEVSKY, *Relative optimization for blind deconvolution*, IEEE Transactions on Signal Processing, Vol. 53, No. 6, pp. 2018 – 2026, June 2005
5. R. BURACHIK, L.M. GRAÑA DRUMMOND, A.N. IUSEM AND B.F. SVAITER, *Full convergence of the steepest descent method with inexact line searches*, Optimization: A Journal of Mathematical Programming and Operations Research, Vol. 32, No. 2, pp. 137 – 146, 1995
6. S. CHOI, S. ONG, J. CHO, C. YOU AND D. HONG, *Performances of neural equalizers on partial erasure model*, IEEE Transactions on Magnetics, Vol. 33, No. 5, pp. 2788 – 2790, September 1997
7. E. CELLEDONI AND S. FIORI, *Neural learning by geometric integration of reduced 'rigid-body' equations*, Journal of Computational and Applied Mathematics (JCAM), Vol. 172, No. 2, pp. 247 – 269, December 2004
8. N. DEL BUONO AND L. LOPEZ, *Runge-Kutta type methods based on geodesics for systems of ODEs on the Stiefel manifold*, BIT Numerical Mathematics, Vol. 41, No. 5, pp. 912 – 923, 2001
9. Z. DING AND Y. LI, *Blind Equalization and Identification*, Marcel Dekker, New York, 2001
10. A. EDELMAN, T.A. ARIAS AND S.T. SMITH, *The geometry of algorithms with orthogonality constraints*, SIAM Journal on Matrix Analysis Applications, Vol. 20, No. 2, pp. 303 – 353, 1998
11. S. ESEDOGLU, *Blind deconvolution of bar code signals*, Inverse Problems, Vol. 20, pp. 121 – 135, 2004
12. E.F.S. FILHO, D.B. HADDAD AND L.A.L. DE ALMEIDA, *Thermal hysteresis characterization through blind deconvolution*, Proceedings of the 17^{th} International Conference on Systems, Signals and Image Processing (IWSSIP 2010, Rio de Janeiro, Brazil, 17-19 June 2010), pp. 352 – 355, 2010

Prepared using acsauth.cls
DOI: 10.1002/acs

13. S. FIORI, *A contribution to (neuromorphic) blind deconvolution by flexible approximated Bayesian estimation*, Signal Processing, Vol. 81, No. 10, pp. 2131 – 2153, September 2001
14. S. FIORI, *A fast fixed-point neural blind deconvolution algorithm*, IEEE Transactions on Neural Networks, Vol. 15, No. 2, pp. 455 – 459, March 2004
15. S. FIORI, *Analysis of modified 'Bussgang' algorithms (MBA) for channel equalization*, IEEE Transactions on Circuits and Systems - Part I, Vol. 51, No. 8, pp. 1552 – 1560, August 2004
16. S. FIORI, *Blind adaptation of stable discrete-time IIR filters in state-space form*, IEEE Transaction on Signal Processing, Vol. 54, No. 7, pp. 2596 – 2605, July 2006
17. S. FIORI, *Geodesic-based and projection-based neural blind deconvolution algorithms*, Signal Processing, Vol. 88, No. 3, pp. 521 – 538, March 2008
18. D. GABAY, *Minimizing a differentiable function over a differentiable manifold*, Journal of Optimization Theory and Applications, Vol. 37, No. 2, pp. 177 – 219, 1982
19. G. GOLUB AND C. VAN LOAN, *Matrix Computations*, The Johns Hopkins University Press, $3^{\rm rd}$ Edition, 1996
20. E. HAIRER, C. LUBICH AND G. WANNER, *Geometric Numerical Integration: Structure-Preserving Algorithms for Ordinary Differential Equations*, Springer Series in Computational Mathematics, $2^{\rm nd}$ Edition, 2006
21. M. LAVIELLE, *A stochastic procedure for parametric and non-parametric estimation in the case of incomplete data*, Signal Processing, Vol. 42, pp. 3 – 17, 1995
22. D.S. LUN, A. SHERRID, B. WEINER, D.R. SHERMAN AND J.E. GALAGAN, *A blind deconvolution approach to high-resolution mapping of transcription factor binding sites from ChIP-seq data*, Genome Biology, Vol. 10, No. 12, pp. 142 – 144, December 2009
23. J. R. MCMAHON, R.K. MARTIN AND S. CAIN, *3D FLASH LADAR range estimation via blind deconvolution*, The Journal of Applied Remote Sensing, Vol. 4, pp. 1 – 28, March 2010
24. A.K. NANDI, D. MÄMPEL AND B. ROSCHER, *Blind deconvolution of ultrasonic signals in nondestructive testing applications*, IEEE Transactions on Signal Processing, Vol. 45, No. 5, pp. 1382 – 1390, May 1997
25. B. NSIRI, J.-M. BOUCHER AND T. CHONAVEL, *Multichannel blind deconvolution application to marine seismic*, Proceedings of the OCEANS 2003 (22-26 Septembre 2003, San Diego, CA, USA), Vol. 5, pp. 2761 – 2766, September 2003
26. D.T. PHAM, *Generalized mutual information approach to multichannel blind deconvolution*, Signal Processing, Vol. 87, No. 9, pp. 2045 – 2060, September 2007
27. B.T. POLYAK, *Newton's method and its use in optimization*, European Journal of Operational Research, Vol. 181, pp. 1086 – 1096, 2007
28. C.-H. QI, K.A. GALLIVAN AND P.-A. ABSIL, *Riemannian BFGS algorithm with applications*, Recent Advances in Optimization and its Applications in Engineering (M. Diehl et al., Ed.s), Part 3, pp. 183 – 192, Springer-Verlag Berlin Heidelberg, 2010
29. M. SPIVAK, *A Comprehensive Introduction to Differential Geometry*, $2^{\rm nd}$ Edition, Berkeley, CA: Publish or Perish Press, 1979
30. O. SHALVI AND E. WEINSTEIN, *Super-exponential methods for blind deconvolution*, IEEE Transactions on Information Theory, Vol. 39, No. 2, pp. 504 – 519, 1993
31. A. SWAMINATHAN, M. WU AND K.J.R. LIU, *Digital image forensics via intrinsic fingerprints*, IEEE Transactions on Information Forensics and Security, Vol. 3, No. 1, pp. 101 – 117, March 2008
32. Y. YANG, *Globally convergent optimization algorithms on Riemannian manifolds: Uniform framework for unconstrained and constrained optimization*, Journal of Optimization Theory and Applications, Vol. 132, No. 2, pp. 245 – 265, February 2007
33. S. YANG, S. BARRIGA, G. ERRY, B. RAMAN, S. RUSSELL, S. MITRA AND P. SOLIZ, *Retinal image deconvolution: Revealing hidden structures and pathology*, Investigative Ophthalmology & Visual Science, 46: E-Abstract 361, 2005
34. B. ZHANG, T. KHAWAJA, R. PATRICK, G. VACHTSEVANOS, M.E. ORCHARD AND A. SAXENA, *Application of blind deconvolution denoising in failure prognosis*, IEEE Transactions on Instrumentation and Measurement, Vol.

DOI: 10.1002/acs

58, No. 2, pp. 303 – 310, February 2009

DOI: 10.1002/acs

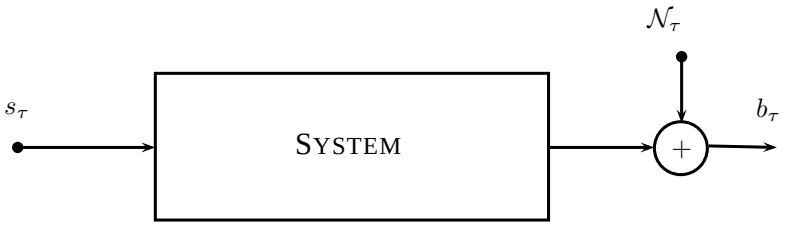

Figure 1. Schematic of a distorting system in a deconvolution problem. The time-sequence s_τ denotes system input, the sequence $\mathcal{N}_\tau$ denotes measurement noise and the sequence b_τ denotes measurable system output.

DOI: 10.1002/acs

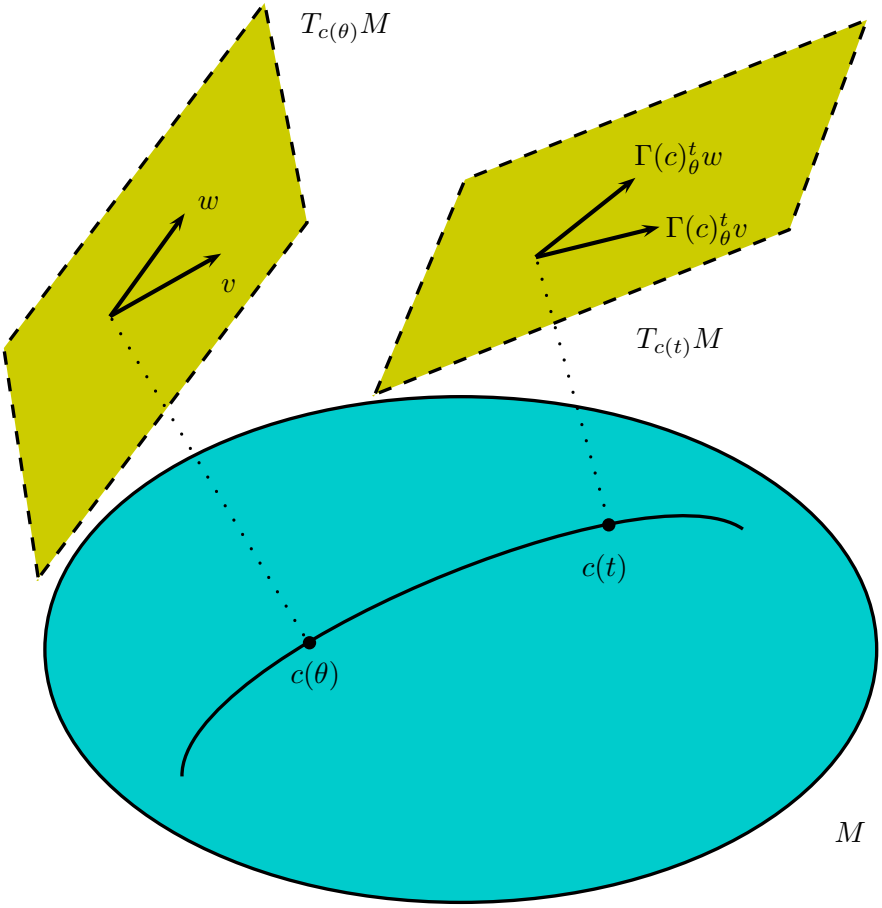

Figure 2. Illustration of the notion of metric parallel translation along a curve c of tangent vectors $v, w \in T_{c(\theta)}M$.

DOI: 10.1002/acs

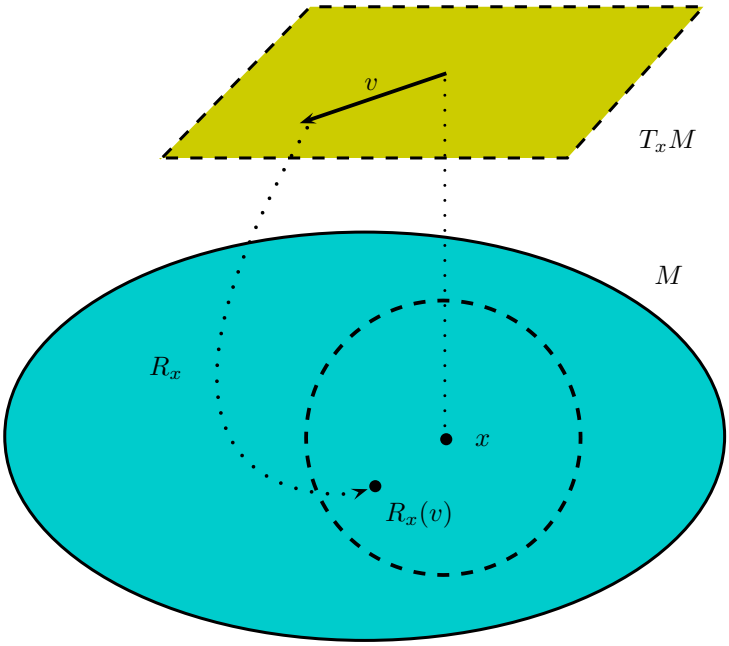

Figure 3. Illustration of the notion of manifold retraction. The figure illustrates the action of a retraction around a point $x \in M$ on a tangent vector $v \in T_xM$. The result $R_x(v)$ lies in a neighborhood of the point x denoted by a dashed circle.

DOI: 10.1002/acs

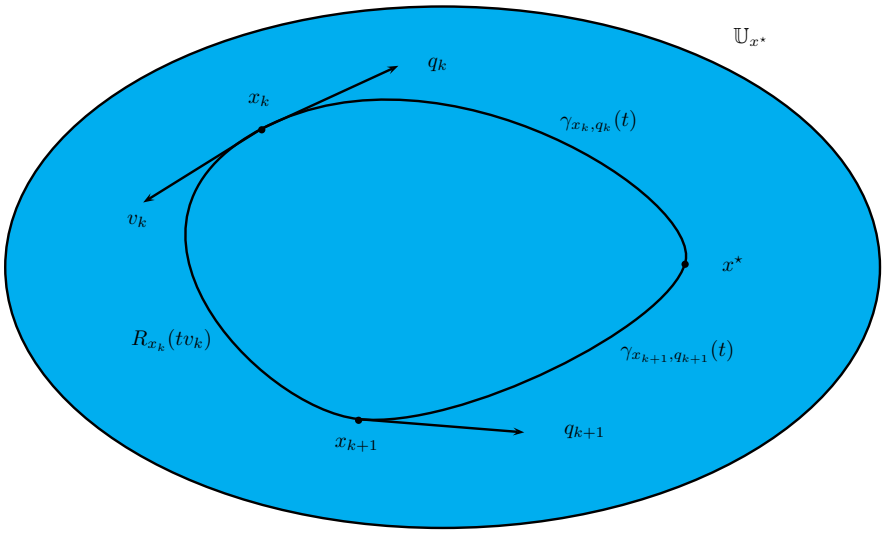

Figure 4. Quantities involved in the convergence analysis of the retracted-Riemannian-Newtonian algorithm. Symbol $x^\star$ denotes a critical point of the function F, while symbols x_k and x_{k+1} denote the current and the next iterate, respectively. The curve $\gamma_{x_k,q_k}(t)$ is the geodesic joining the iterate x_k with the critical point while the curve $R_{x_k}(tv_k)$ joins the current iterate with the next iterate. It is assumed that the succession x_k belongs to a normal neighborhood $\mathbb{U}_{x^\star}$ which surrounds the points in the figure.

DOI: 10.1002/acs

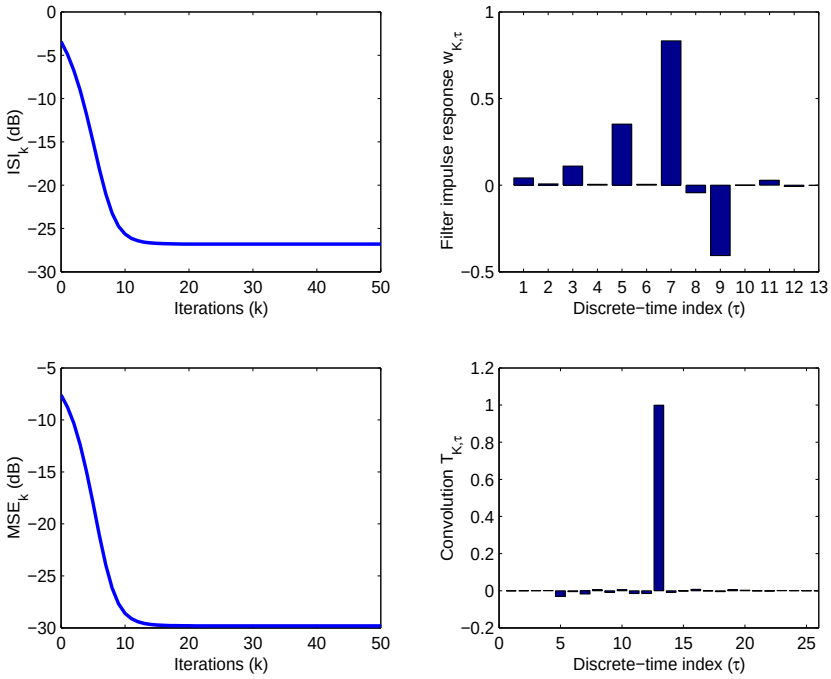

Figure 5. Experiments on noiseless sampled telephonic channel. Results obtained with the geodesic-based Riemannian-Newtonian blind deconvolution algorithm: Performance indices and adapted inverse filter.

DOI: 10.1002/acs

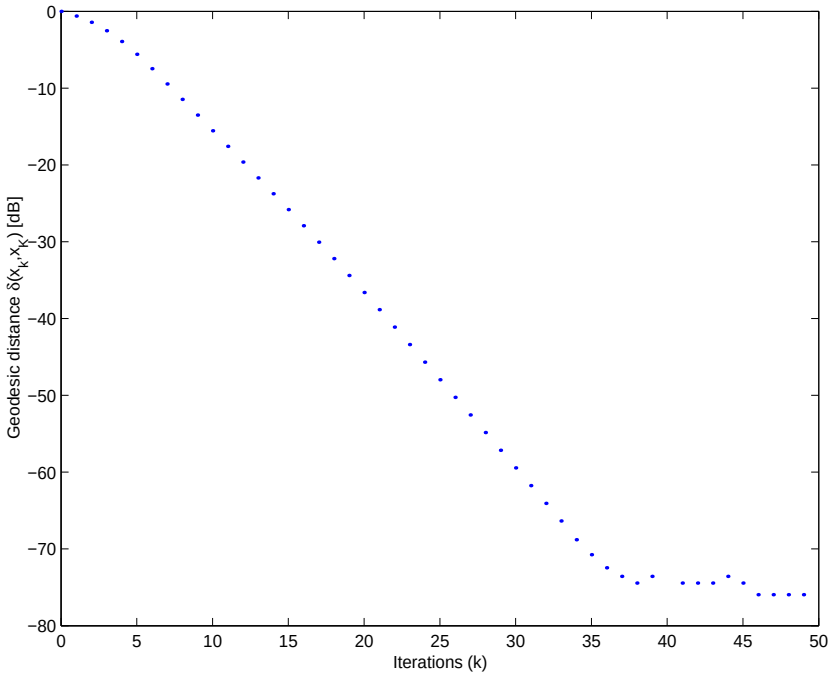

Figure 6. Experiments on noiseless sampled telephonic channel. Results obtained with the geodesic-based Riemannian-Newtonian blind deconvolution algorithm: Distance-sequence to illustrate the rate of convergence.

Prepared using acsauth.cls
DOI: 10.1002/acs

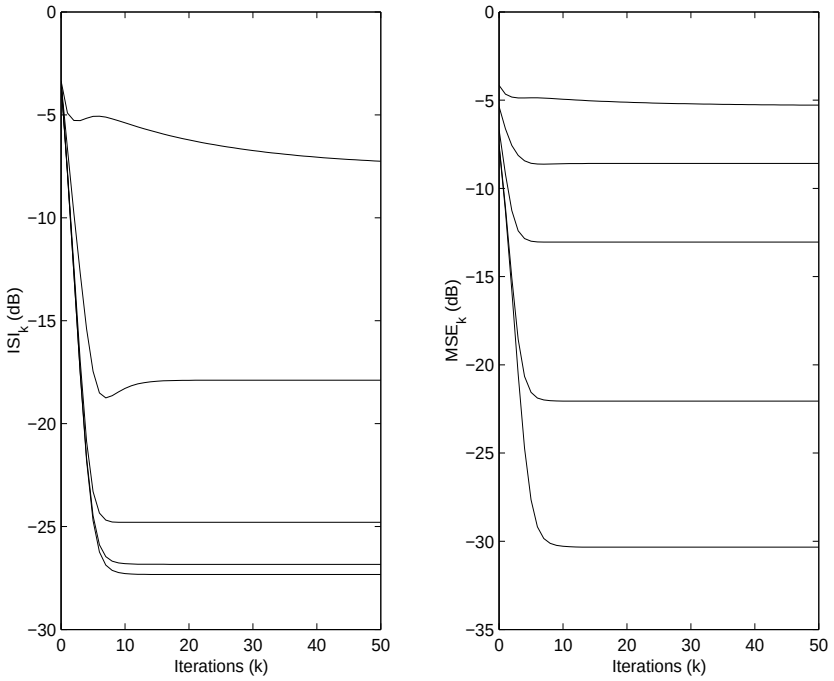

Figure 7. Experiments on noisy sampled telephonic channel. Performance indices pertaining to the geodesic-based Riemannian-Newtonian blind-deconvolution algorithm for four different values of the SNR. The correspondence of the curves with the SNR levels is: Lower asymptotic values correspond to higher SNR levels.

DOI: 10.1002/acs

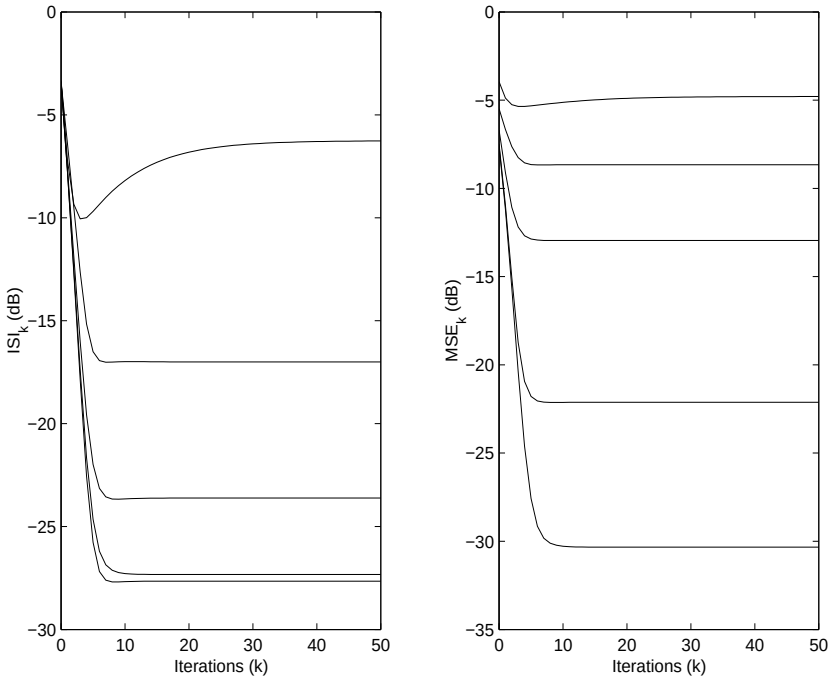

Figure 8. Experiments on noisy sampled telephonic channel. Performance indices pertaining to the retraction-based Riemannian-Newtonian blind-deconvolution algorithm for four different values of the SNR. The correspondence of the curves with the SNR levels is: Lower asymptotic values correspond to higher SNR levels.

Prepared using acsauth.cls
DOI: 10.1002/acs

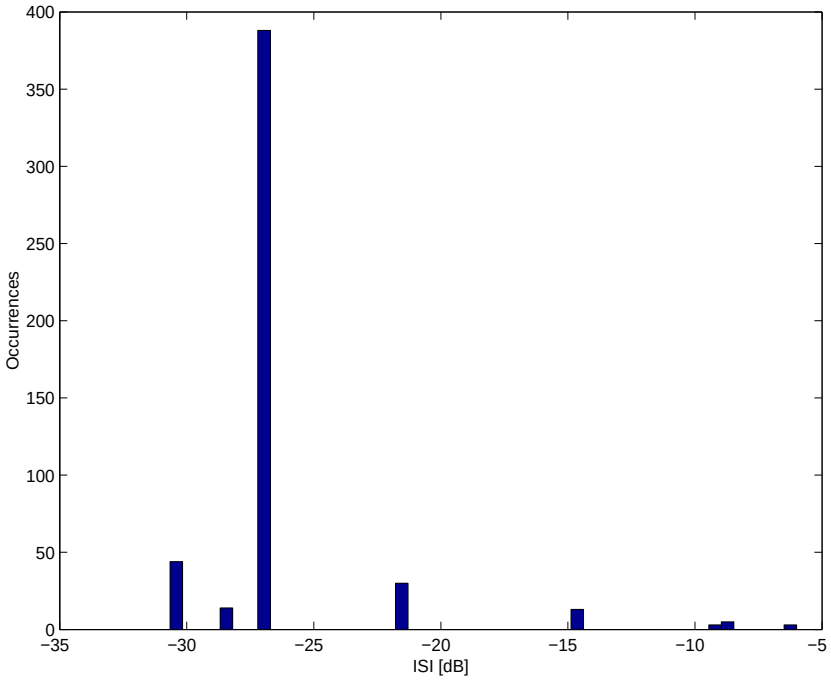

Figure 9. Analysis of the dependence of the optimization ability of a projection-based Riemannian-Newtonian algorithm from the initial point. Analysis conduced over 500 indpendent trials.

Prepared using acsauth.cls
DOI: 10.1002/acs

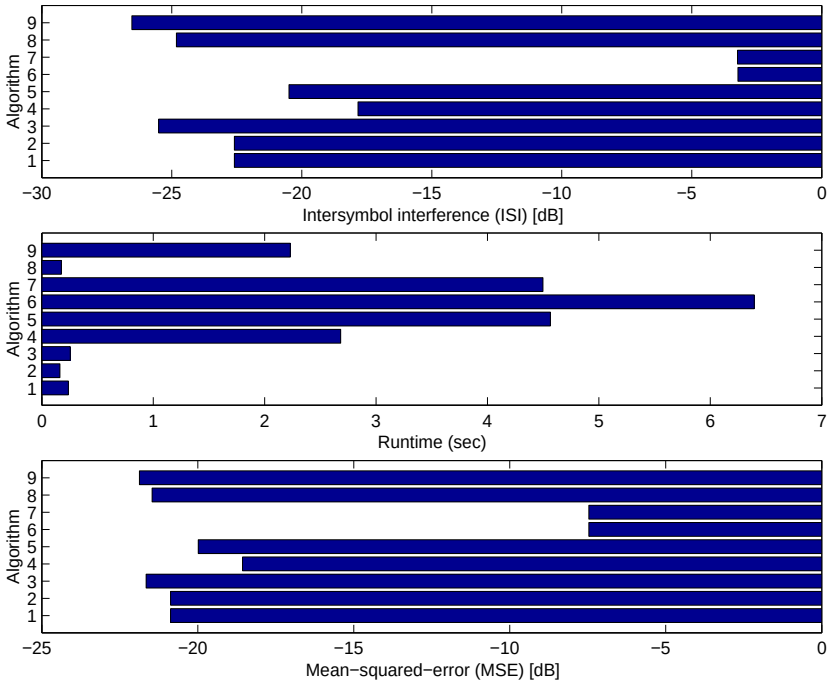

Figure 10. Comparative analysis on a noisy sampled telephonic channel. Comparison of results obtained with the geodesic-based Riemannian-Newtonian algorithm (1), the geodesic-based Riemannian-gradient algorithm (2), the retraction-based Riemannian-Newtonian algorithm (3), the enhanced Bussgang algorithm (4), the Bussgang algorithm (5), the Bussgang algorithm with natural gradient (6), the enhanced Bussgang algorithm with natural gradient (7), the fixed-point enhanced Bussgang algorithm (8) and the fast quasi-maximum-likelihood relative Newton algorithm (9).

Prepared using acsauth.cls
DOI: 10.1002/acs

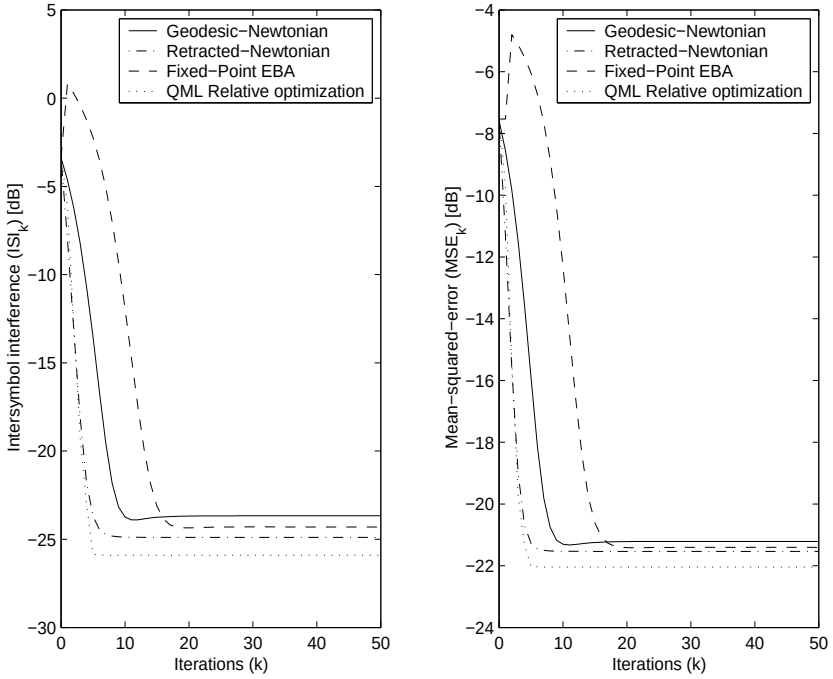

Figure 11. Comparative analysis on a noisy sampled telephonic channel. Comparison of ISI and MSE adaptation curves obtained with the geodesic-based Riemannian-Newtonian algorithm, the retraction-based Riemannian-Newtonian algorithm, the fixed-point enhanced Bussgang algorithm and the fast quasi-maximum-likelihood relative Newton algorithm.

Prepared using acsauth.cls
DOI: 10.1002/acs